

Journal Pre-proof

Targeting RAS-RAF pathway significantly improves antitumor activity of Rigosertib-derived platinum(IV) complexes and overcomes cisplatin resistance

Zhikun Liu, Meng Wang, Hengshan Wang, Lei Fang, Shaohua Gou



PII: S0223-5234(20)30236-1

DOI: <https://doi.org/10.1016/j.ejmech.2020.112269>

Reference: EJMECH 112269

To appear in: *European Journal of Medicinal Chemistry*

Received Date: 11 December 2019

Revised Date: 22 March 2020

Accepted Date: 22 March 2020

Please cite this article as: Z. Liu, M. Wang, H. Wang, L. Fang, S. Gou, Targeting RAS-RAF pathway significantly improves antitumor activity of Rigosertib-derived platinum(IV) complexes and overcomes cisplatin resistance, *European Journal of Medicinal Chemistry* (2020), doi: <https://doi.org/10.1016/j.ejmech.2020.112269>.

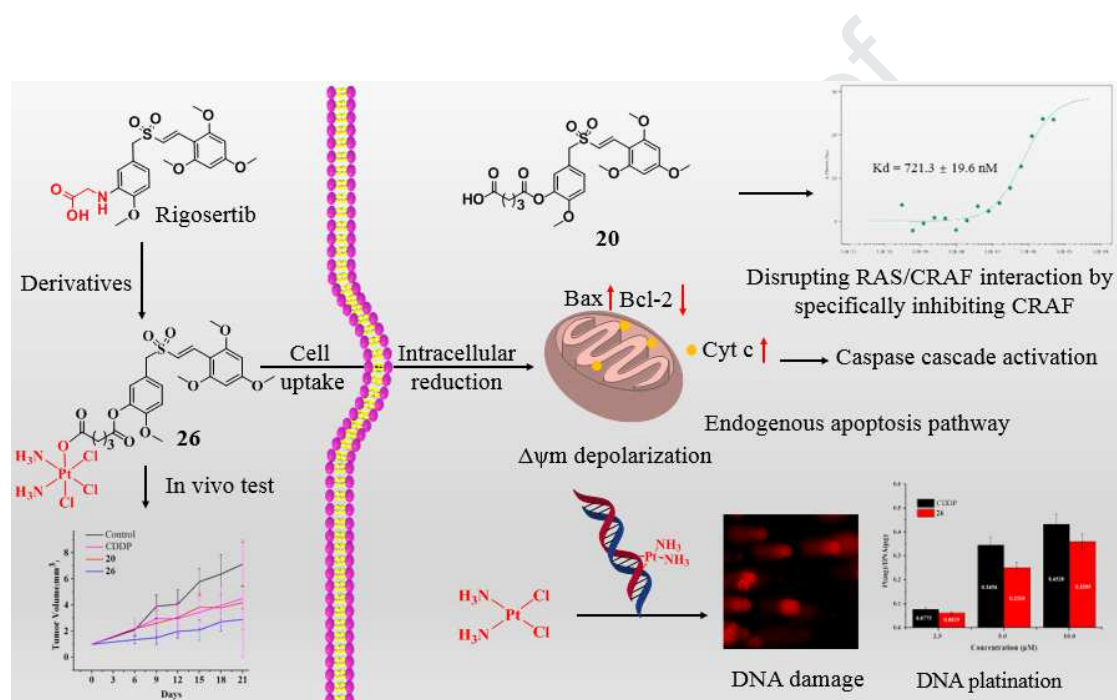
This is a PDF file of an article that has undergone enhancements after acceptance, such as the addition of a cover page and metadata, and formatting for readability, but it is not yet the definitive version of record. This version will undergo additional copyediting, typesetting and review before it is published in its final form, but we are providing this version to give early visibility of the article. Please note that, during the production process, errors may be discovered which could affect the content, and all legal disclaimers that apply to the journal pertain.

© 2020 Published by Elsevier Masson SAS.

Graphical abstract

Targeting RAS-RAF pathway significantly improves antitumor activity of Rigosertib-derived platinum(IV) complexes and overcomes cisplatin resistance

Zhikun Liu^{a,b,1}, Meng Wang^{c,1}, Hengshan Wang^c, Lei Fang^{a,b,*}, Shaohua Gou^{a,b,*}



Total 11 Pt(IV) compounds by introducing ON013100 onto hydroxyl ligand of Pt(IV) complexes derived from CDDP and oxaliplatin through ester bond were designed and synthesized. The conjugate **26** could effectively release Pt(II) complexes and RAS analogues to exert anti-tumor activity in novel pathway. The following biological studies revealed that **26** could efficiently disrupt the interaction between RAS and CRAF by specifically interacting with CRAF. Furthermore, **26** could apparently induce DNA damage and initiate endogenous caspase apoptosis pathway. Moreover, **26** also showed excellent anti-tumor effect in vivo. All the findings suggested that **26** may be considered as a novel antitumor candidate for further exploration.

Targeting RAS-RAF pathway significantly improves antitumor activity of Rigosertib-derived platinum(IV) complexes and overcomes cisplatin resistance

Zhikun Liu^{a,b,1}, Meng Wang^{c,1}, Hengshan Wang^c, Lei Fang^{a,b,*}, Shaohua Gou^{a,b,*}

^a Jiangsu Province Hi-Tech Key Laboratory for Biomedical Research, Southeast University, Nanjing, 211189, China

^b Pharmaceutical Research Center, School of Chemistry and Chemical Engineering, Southeast University, Nanjing 211189, China

^c State Key Laboratory for the Chemistry and Molecular Engineering of Medicinal Resources, School of Chemistry and Pharmaceutical Sciences of Guangxi Normal University, Guilin, 541004, China

Abstract

RAS-RAF pathway presents a valuable target for the cancer treatment due to its important roles in the regulation of tumor proliferation, apoptosis and the obtained resistance. To explore such target a RAS/CRAF interference agent, was therefore conjugated with Pt(IV) prodrugs via ester bond, resulting in total eleven multifunctional Pt(IV) complexes. The complexes could target genomic DNA and disrupt the signaling transduction from RAS protein to CRAF so that block the mitogen-activated protein kinase (MAPK) signaling pathway. Experiments in vitro indicated that all of the Pt(IV) complexes showed potent anti-tumor activity with IC₅₀ values ranged from 8 nM to 22.55 μM, which were significantly improved as compared with cisplatin (CDDP) whose IC₅₀ values ranged from 5.45 μM to 9.05 μM. Among them, **26** exerted the best anti-tumor activity in vitro, which not only exhibited excellent cytotoxicity against normal tumor cells, but also against CDDP-resistance cell lines (e.g. A549/CDDP and SKOV-3/CDDP). Importantly, **26**

¹These authors contributed equally.

* Corresponding authors

E-mail: lei.fang@seu.edu.cn (L. Fang); sgou@seu.edu.cn (S. Gou)

only showed little effect on normal cell lines such as HUEVC and LO2. Besides, the following biological mechanisms studies demonstrated that **26** could efficiently enter A549 cells, significantly arrest cell cycle at G2/M phase, disrupt the signaling pathway and trigger endogenous caspase apoptosis pathway. Furthermore, results of a xenograft subcutaneous model of A549 tumor showed that **26** could effectively decrease tumor growth rates without causing loss of bodyweight.

Keywords: Pt(IV) complexes, RAS-RAF interaction disruptors, RAS-signaling and mitochondrial apoptosis pathways, Overcoming CDDP resistance.

1. Introduction

RAS proteins are members of membrane-bound guanine nucleotide-binding proteins which have a crucial role in regulation of transducing extracellular signals into diverse physiological activity, including cell proliferation, differentiation and survival [1-4]. RAS functions as molecular switches in regulation of GDP/GTP transformation with the help of extracellular signals and subsequently results in activation of several downstream cascades, including RAF-MEK-ERK pathway [5-8]. Upon extracellular stimulus (e.g. GTPase-activating proteins, GAPs), RAS switches from active GTP-bound signaling state to inactive GDP-bound signaling state with the function of its intrinsic GTPase [9,10]. However, mutations frequently occurred in *HRAS*, *NRAS* or *KRAS* (three isoforms of the RAS family) – mutating about 20% - 30% of all human tumors [11,12]. The mutation of RAS results in the attenuation GTPase activity or insensitivity of GAPs, which in turn constitutively activates RAS proteins, therefore, leading to cell growth out of control and induction of carcinogenesis [13,14]. These facts indicate that RAS has played important roles in occurrence and development of human cancer, thus should be a crucial target for the cancer treatment. In the past decades, the development of RAS inhibitors proved to be challenging due to the lack of druggable pockets [1,15-17]. Moreover, many tumors frequently develop sharing the same signaling pathway, although lack RAS mutations

[18]. Therefore, to develop a novel approach to inhibit mutant RAS-mediated cancer is in great need.

Due to the enormous obstacles in seeking RAS inhibitors, exploiting therapeutic agents which can disrupt RAS signaling pathways transduction provides a novel therapy to treat mutant RAS-driven cancers [16,19]. As downstream effectors of RAS proteins, proteins serine/threonine kinase RAF are activated by GTP-bound RAS and subsequently activate mitogen-activated protein kinase kinases 1 and 2 (MEK1 and MEK2) to regulate cell proliferation and apoptosis [18, 5-8]. Therefore, it should be valuable to disrupt the signaling transduction between RAS proteins and RAF proteins to achieve the same efficiency of RAS inhibitors in treatment of cancers. Previously, Rigosertib (**Figure 1**) which possessed specific styrylbenzylsulfone structures acted as RAS-mimetic to block signaling transduction to RAS downstream effectors [15, 20, 21]. Interestingly, ON 013100 (**Figure 1**) also contained the same specific structure, which suggested that it may probably possess the same effect on disrupting the signaling transduction between RAS and CRAF.

Cisplatin, carboplatin and oxaliplatin (**Figure 1**) were FDA-approved Pt(II) agents which were widely used in clinical chemotherapy [22-26]. Despite the excellent anti-tumor activity in vitro and in vivo, toxicity, acquired or inherent drug-resistance occurred frequently, limiting their chemotherapeutic efficiency greatly [27-30]. Pt(IV) complexes, possessing insert physicochemical properties compared to Pt(II) complexes, were considered as promising candidates for overcoming the drawbacks of classical platinum(II) drugs [31-34]. The desired biological properties, such as lipophilicity, tumor-targeting property and improved cellular uptake, could be obtained from the structural modification of the two extra ligands [35-39]. Besides, the insert Pt(IV) complex could release Pt(II) with the help of reduction agents of intracellular reducing substance (e.g. ascorbic acid and GSH, etc.). Thus, the Pt(IV) complex could be considered as the prodrugs of the classic Pt(II) complexes. In this context, it will be interesting to introduce the RAS/CRAF interference agent such as ON 013100 to the two extra ligands of Pt(IV) complex. We and others have employed

one strategy by construct insert Pt(IV) prodrugs which could release Pt(II) with the help of reduction agents [28, 33-35]. In our assumption, the resulting Pt(IV) complexes may act as interference agents to disturb the signaling transduction between RAS protein and RAF protein, and the block of the RAS-RAF pathway may be beneficial for antitumor activity of Pt-based drugs since such complex could simultaneously act on two different targets. More importantly, the block of the RAS-RAF pathway could help to overcome the resistance to platinum-based drugs as reported from former studies.

Based on the information aforementioned, we here constructed total 11 Pt(IV) compounds by introducing ON013100 into hydroxyl ligand of Pt(IV) complexes derived from CDDP and oxaliplatin through ester bond. We expected that the conjugates could be transported into tumor cells, and then be reduced in cells to release their corresponding Pt(II) complexes and RAS analogues to exert anti-tumor activity in novel pathway.

2. Results and discussion

2.1 Chemistry

The synthetic routes for preparation of target Pt(IV) compounds were shown **Scheme 1** and **2**. Compound **9** was obtained following previously reported procedures [40,41]. In detail, compound **9** was reacted with ethyl bromoacetate in the presence of anhydrous K_2CO_3 and catalytic amount of KI, to get compound **10**. Complete hydrolysis of **10** in a solution of MeOH/H₂O with LiOH·H₂O as base gave compound **11**. Compounds **19** and **20** were obtained by acylation of **9** with succinic anhydride or glutaric anhydride in the presence of anhydrous K_2CO_3 . Finally, condensation reaction was carried out between **11/19/20** and **15/16/17/18** in DMF using TBTU as condensation agent and Et₃N as organic base to give the final target Pt(IV) compounds **12-14** and **21-28**, respectively.

2.2. In vitro anti-tumor activity assay

The anti-proliferative effects of the target Pt(IV) compounds on tumour cells including A549 (human non-small cell lung cancer) cells, OVCaR-3 (human ovarian

cancer) cells, SGC-7901 (human gastric cancer) cells and HCT-116 (human colon cancer) cells were firstly measured in vitro. The 50% growth inhibitory concentration (IC_{50}) values were calculated and summarized in **Table 1** after 72 h co-incubation with these compounds. All the compounds showed apparent cytotoxic activity toward the selected human tumour cells, with IC_{50} values ranging from 8 nM to 22.55 μ M. However, the compounds using glycolic acid as the linker (i.e. compounds **12**, **13**, **14**) showed relative low cytotoxicity (IC_{50} values ranged from 3.82 to 22.55 μ M) as compared with the positive control **9** (IC_{50} values ranged from 0.026 to 0.031 μ M) and other target compounds. The low cytotoxicity may be attributed to stability of ether bond which could hardly be hydrolysed to release ON013100. In contrast, compounds **19-28**, which used cleavable phenolic ester bond to connect Pt(IV) complexes and ON013100, obtained excellent anti-tumor activity (IC_{50} values ranged from 8 to 39 nM) against all cancer cells, over 100-fold higher than that of CDDP and oxaliplatin. In particular, **26** was most effective in inhibiting A549 cells proliferation with IC_{50} value of 8 nM, which was even over 3-fold lower than that of ON 013100 (IC_{50} was 29 nM).

2.3. *In vitro* cytotoxicity assays against cisplatin-resistant cells and normal cells

The acquired drug-resistance occurred in therapy severely hindered CDDP to fight cancer, therefore easily caused the treatment failure. It is believed that the overexpressing P-glycoprotein is responsible for the drug-resistance since it could pump out the therapeutic drug out of the cells and finally reduce the intracellular drug concentrations [42-44]. Previously, Reddy and co-workers reported that ON013100 was active against a wide variety of human tumor cell lines, including multidrug-resistance tumor cell lines [40,41]. So it may be possible that our target compounds may also overcome the multidrug resistance. In consideration of excellent anti-tumor activity of **26**, we further determined the activity of **26** against CDDP-resistance non-small lung cancer (A549/CDDP) cells and CDDP-resistance ovarian cancer (SKOV-3/CDDP) cells, selecting CDDP and **20** as the controls. Besides, to determine the cytotoxicity of **26** to human normal cell lines, human

umbilical vein endothelial cells (HUVEC) and normal liver (LO2) cells were also used for the study. The IC_{50} values were calculated and summarized in **Table 2**. Cell viability measurements showed that CDDP showed moderate cytotoxicity to A549 cells and SKOV3 cells (IC_{50} values were 8.22 μ M and 7.45 μ M, respectively), but only weak activity to A549/CDDP (IC_{50} value was 34.55 μ M) and SKOV-3/CDDP (IC_{50} value was 40.55 μ M), with resistance factor as 4.2 and 5.4, respectively. In contrast, both normal and CDDP-resistant tumor cells were almost equally sensitive to **20** and **26** when those tumor cells were co-incubated with **20** or **26**, with RF values of 1.3, 1.2, 1.1 and 1.6, respectively. The results strongly support that our target compounds could overcome the CDDP-resistance. Interestingly, the RF values raised slightly when CDDP-resistance cells were treated with combination administration of CDDP and **20**, indicating that our target compounds had better performance than the combination administration of the active components. More importantly, the combination administration caused obviously toxicity to normal cell lines (IC_{50} values of 0.45 μ M and 1.45 μ M for HUVEC and LO2, respectively), while **20** and **26** showed only a moderate cytotoxicity to the normal cells with IC_{50} values ranging from 7.86 to 182.80 μ M, more than 100-fold higher than the IC_{50} values for tumor cells. Obviously, our target compounds had much wider therapeutic window than the combination administration. Therefore, the potent activity of **26** to both normal and resistant tumor cells as well as the excellent safety profile made **26** valuable for the following bioactivity studies.

2.4. HPLC analysis of activation of 26 by reduction

Based on the concept of prodrug strategy, compound **26** could be reduced by intracellular reducing substance to release their biological compound **20** and the corresponding Pt(II) complex [42-44]. Therefore, we used HPLC chromatography to investigate the stability of compound **26** in physiological condition (PBS, pH = 7.4) and reductive (i.e. ascorbic acid) condition. Compound **20** or ascorbic acid was used as reference to match the peaks appeared in the chromatography of **26** after the treatment. The results were shown in **Figure S1** (see supporting information). It was

found that **26** was stable within 36 h in PBS (pH =7.4). However, when treated with ascorbic acid (3 equiv.) compound **26** gradually decomposed as reflected by the decreasing peak of compound **26** and the increasing peak which appeared just right at the position of compound **20**, indicating that compound **26** was successfully reduced to its corresponding product compound **20**. Surprisingly, no peak of cisplatin was detected, perhaps for its weak chromophore under this test condition [37-39]. In all, compound **26** was stable under physiological condition and could be effectively reduced to compound **20** within 7 h when exposed to ascorbic acid. Moreover, HR-MS assays were performed to investigate the reduction character of the Pt(IV) complex. After 24 h co-incubation with **26**, A549 cells were lysed and the lysates were filtered with millipore filtration (0.22 μm). As shown in **Figure S1F**, '[CDDP+NH4] +=317.9834' could be detected clearly in A549 cells lysates, which revealed the existence of CDDP in A549 cells and validated the reduction of **26**. This result, together with the finding of the HPLC analysis, gave solid evidences of the reduction of the Pt(IV) complex. Besides, we also tested the stability of **26** in DMSO- d_6 solution in every 24 h for one week. The results in **Figure S1G** showed that **26** was stable in DMSO- d_6 solution at least in 7 days and the characteristic peaks (6.30-6.12, 6H) of cisplatin (oxidation state) in $^1\text{H-NMR}$ spectra showed no significant change. Besides, the NMR spectrum in DMSO- d_6 of **26** showed no difference with that of DMF- d_7 (**Figure S1G**).

2.5. Cellular uptake, DNA platination and gel electrophoretic assays

According to previous reports [38, 39], increased cellular uptake plays important roles in the improved activity of the Pt(IV) complexes. Therefore, the most active compound **26** was selected to investigate whether the intracellular Pt content was increased. A549 cells were treated and co-incubated with **26** (5 and 10 μM) for 12 hours, digested with 65% HNO_3 and measured the Pt content with inductively coupled plasma mass spectrometry (ICP-MS) [37-39]. Similarly, CDDP with the same concentrations were carried out as positive control groups. As shown in **Figure 2**, total 56 ng/ 10^6 cells Pt were found when the cells were treated with 5 μM CDDP, and

the Pt content was increased to 114 ng/10⁶ cells when the concentration of CDDP was enhanced to 10 μ M. When compound **26** was employed in the test, much higher Pt accumulation was observed. At equal dosage, the intracellular Pt content of **26** group was at least 2-fold higher than that of CDDP group. The enhanced cellular uptake could be attributed to the hydrophobic ligands of the Pt(IV) complex which increased the lipophilicity of the platinum complex, therefore, contributing to the transportation through cell membrane and making **26** exerted better cytotoxicity than CDDP.

The enhanced cellular uptake of **26** motivated us to investigate whether the intracellular **26** shared the similarly DNA-binding properties like cisplatin. Therefore, we firstly performed ICP-MS analysis to determine the platinum contents in DNA extracted from A549 cells after 12 h co-incubation with CDDP (2.5, 5 and 10 μ M) and **26** (2.5, 5 and 10 μ M). As revealed in **Figure S2B**, the Pt content in DNA accordingly increased as the dosage of CDDP and **26** increased from 2.5 to 10.0 μ M. The results clearly indicated that DNA in A549 cells was platinated after 12 h co-incubation with **26**. It was also found that the contents of platinum in A549 cells were in a dose-dependent manner (**Figure S2B**). Interestingly, the extent of DNA platination in **26**-treated A549 cells was lower than the CDDP-treated group at the same concentration. This may be attributed to the fact that the Pt(IV) prodrug need to be reduced to the Pt(II) form to interact with DNA and this process was revealed previously in **Figure S1E**.

Moreover, to further investigate the effect of **26** on biological function of DNA, gel electrophoretic assays of **26** interacting with pBR322 plasmid DNA under the reduction of ascorbic acid were also carried out. Briefly, pBR322 plasmid DNA was co-incubated for 3 h at 37 °C with increasing concentration of CDDP (1.25, 2.5, 5, 10, 20 and 40 μ M) or **26** (1.25, 2.5, 5, 10, 20 and 40 μ M) which was pre-treated with ascorbic acid for 7 h at 37 °C and analysed with electrophoresis in agarose gel. Similarly, **20** and **26** without the pre-treatment with ascorbic acid at various concentrations were used as control groups. From the electrophoretograms shown in **Figure S2C–S2F**, we found that the untreated pBR322 plasmid DNA in each group

mainly presented in two states, form I bands (closed circular) and form II bands (open circular) [45]. However, the mobility of form I bands of pBR322 plasmid DNA decreased gradually when co-incubated with CDDP and **26** (pre-treated with ascorbic acid), especially at the concentrations of 20 or 40 μM . On the contrary, the results in **Figure S2C** and **S2D** indicated that the mobility of form II bands of pBR322 plasmid DNA was accelerated. Naturally, the bands of coalescence in electrophoretograms were interpreted as a strong unwinding of the supercoiled DNA [46]. Not surprisingly, both **20** or **26** without the pre-treatment with ascorbic acid did not interacted with DNA (**Figure S2E** and **S2F**). Therefore, these findings proved that **26** could bind to DNA by inducing DNA platination, change the conformations of plasmid DNA and consequently affect the biological function of DNA, whereas **20** did not show such activity. Therefore, those results mentioned above proved that **26** could induce DNA damage and disrupt DNA biological function in A549 cells.

2.6. Apoptosis test

The strong antiproliferative activity of compounds **19-26** raised a question whether the inhibition of growth of tumour cells was promoted by apoptosis. Therefore, we chose **26** to assess apoptosis of A549 cells by annexin V–propidium iodide assays. In early apoptosis, phosphatidylserine (PS) jumped into outer leaflet of cell membrane and could be identified and marked with annexin V–FITC, which was shown in Q3 of cytometry assay. In contrast, necrotic cells or late apoptotic were both stained with PI, which was showed in Q1 and Q2. Similarly, normal cells were shown in Q4. As shown in **Figure 3**, for the control group few cells were in apoptotic state (4.57%). In contrast, the apoptosis population was significantly increased to 45.4% after treatment with **26** (2 μM) for 24 h and further increased to 52.5% when the concentration of **26** was increased to 5 μM . As far as CDDP (5 μM) was concerned, it only induced apoptosis with a population of 15.43 %, clearly lower than that of **26**. Similarly, **20** also could induce apoptosis in a dose-dependent manner but was more moderate than **26**. This finding is similar to their performance in the cytotoxicity assay in **Table 1**. Thus, a conclusion can be drawn that **26** could clearly

induce cell apoptosis and this ability closely correlates to its anti-tumor activity. Therefore, in order to obtain better interpretation of design concepts and quickly reveal the related biological mechanism, we chose the **20** (2 μ M or 5 μ M) and **26** (2 μ M or 5 μ M) of 24 h treatment for further studies.

2.7. Effect of **26** on RAS/RAF interaction and MEK/ERK activation

Previously, Reddy and co-workers reported that Rigosertib could act as RAS analogues to bind to RAS effectors, resulting in their inability to bind to RAS, disrupting RAF activation, and inhibiting activation of the RAS-RAF-MEK pathway [15]. Because of the similarity in structure between **20** and Rigosertib, we hypothesized that **20** and its relative Pt(IV) prodrug **26** could show the same biological activity. Therefore, to determine whether **26** disturbed the interaction of RAS and RAF, cell lysates of A549 cells that were pre-incubated with **20** (5 μ M) or **26** (5 μ M) for 24h were incubated with VE-cadherin (anti-RAS). The resulting complexes were precipitated with protein G agarose and subjected to western blotting to determine the levels of its associated p-CRAF. As shown in **Figure 4A** and **4B**, treatment of A549 cells with **20** and **26** induced significant decrease of the ratio of p-CRAF between input groups and IP groups in comparison with untreated groups, which elucidated that both **20** and **26** could inhibit the formation of p-CRAF. Besides, treatment of cell lysates with protein G agarose that contained anti-RAS antibody resulted in disability of CRAF protein to bind to RAS protein, which was observed apparently in input group in **Figure 4A** and **Figure 4B**. These results supported our hypothesis that **26** did inhibit the formation of RAS/CRAF complexes.

In order to further investigate whether **26** directly targeted RAS protein or CRAF protein or both, we further carried out microscale thermophoretic (MST) assays and cellular thermal shift assays (CETSA). As illustrated in **Figure S3E** and **S3F**, **26** could bind to CRAF RBD protein with high affinity constant (Kd value was 3.93 μ M) while **26** could not bind to KRAS (**Figure S3C** and **Figure S3D**) even when the initial concentration of **26** was increased to 62.5 μ M, indicating that **26** disrupted the signaling transduction between RAS and CRAF by binding to CRAF rather than

RAS or both [15-17]. As an analogue of Regosertib, **20** could also bind to CRAF RBD protein with Kd value of 721.3 nM (**Figure S3A and S3B**). Moreover, results of CETSA shown in **Figure S4A and S4B** revealed that the melting temperature of CRAF RBD protein from 47 to 67 °C significant increased, especially for CRAF RBD protein at the temperature from 47 to 55 °C. It was found that more than 90% of protein remained with the rising of temperature from 47 to 55 °C. As for the negative group, the level of CRAF remaining in the soluble fraction quickly decreased when the A549 cell lysates were heated from 47 to 67 °C. This phenomenon suggested that both **20** and **26** could bind and stabilize CRAF protein. Thus, both MST and CETSA assays showed that **26** was able to engage CRAF protein rather than RAS protein.

With these results obtained, we further studied the effect of **26** on the MAPK signals by measuring phosphorylation of MEK (p-MEK) and ERK (p-ERK). Briefly, cell lysates collected from A549 cells that were co-incubated with **20** (2 µM and 5 µM) and **26** (2 µM and 5 µM) for 24 h were subjected to western blot to evaluated the levels of p-MEK and p-ERK. CDDP (5 µM) and DMF were used as controls, respectively. As expected, the results in **Figure 4C and 4D** showed that treatment with both **20** and **26** led to reduced p-MEK and p-ERK levels with dose-dependent manner. On the other hand, when A549 cells were treated with CDDP (5 µM), little effect on p-MEK or p-ERK were observed. In sum, these results supported that **26** could inhibit MAPK signals pathway by inhibiting phosphorylation of MEK/ERK.

2.8. Effect on cell cycle arrest

As compound **26** was found to be able to induce cell apoptosis, it is necessary to investigate its effect on tumor cell cycle. Therefore, **26** and its corresponding ligand **20** were chosen to carry out florescence activated cell sorting (FACS) analysis with A549 cells, using DMF and CDDP as negative and positive control respectively. The results were shown in **Figure 5**. After 24 h co-incubation with the tested compound, we found that **26** did affect the progression of cell cycle. The results in **Figure 5** showed that the positive drug CDDP caused a moderate arrest in S phase as compared with cells without any treatment. However, cells cycle block induced by **26** or **20**

were completely different from that of CDDP. A549 cells treated with **20** or **26** were gradually accumulated in G2/M phase of the cell cycle (cell population of G2/M phase increased to 39.04%, 67.36% for 2 μ M and 5 μ M of **26**; 35.60%, 60.32% for **20** when compared with 6.03% of negative control) and appeared to be unable to exit from this phase, resulting in the activation of apoptotic pathways, as reflected with the increased p53 and cleaved PARP proteins (see western blotting experiments) which was a marker of caspase activation. In conclusion, compound **26** could induce A549 cells apoptosis by blocking cell cycle at G2/M phase just like **20** did.

2.9. DNA damage induced by **26**

To investigate whether **26** could induce DNA damage, comet assays and relative western blotting assays were performed. Briefly, A549 cells were co-incubated with **20** (5 μ M), **26** (5 μ M) or CDDP (5 μ M) for 24 h and used for further biological studies. As revealed in **Figure 6**, DNA damage occurred clearly in both CDDP-treated and **26**-treated groups, which was characterized by the tail DNA. Usually, tail DNA was in positive correlation with the degree of DNA damage. In our test **26** induced longer and more tail DNA than both CDDP-treated and **20**-treated groups, which indicated that **26** induced much stronger DNA damage after 24 h co-incubation with A549 cells. The finding was further confirmed by the fact that **26** induced high generation of phosphorylation H2AX (γ H2AX) in A549 cells, which was a biomarker of double-strand breaks (DSBs) [47-49] (**Figure S5**). Moreover, the expression of γ H2AX induced by **26** was in a dose-dependent manner as compared with control group. Naturally, the DNA damage could induce the up-regulation expression of p53 protein [38, 50, 51]. Results in **Figure S5** illustrated that **20** (5 μ M), **26** (5 μ M) or CDDP (5 μ M) enhanced the level of p53 in A549 cells after 24 h co-incubation. In sum, **26** could significantly induce DNA damage with the characteristics of platinum drugs by leading to endogenous DSBs.

2.10. Reactive oxygen species (ROS) assays

After knowing that **26** showed the most potential anti-tumor activity, we carried out studies to investigate the intracellular induction mechanism of apoptosis. Previous reports have proved that metal complexes exerted anti-tumor efficiency through

increasing generation of ROS [52, 53]. Therefore, we investigated whether treatment with **26** led to significant production of ROS in A549 cells. To evaluate the level of ROS accumulation, A549 cells were incubated with **20** (5 μ M), **26** (5 μ M) or CDDP (5 μ M) for 24 h, using dichloro-dihydro-fluorescein diacetate (DCFH-DA) as the ROS probe and observed with fluorescence microscopy. Results in **Figure 7** showed that **26** (5 μ M) treated A549 cells produced a remarkable increase in generation of ROS (65.56% population of whole A549 cells), which led to irreversible cell death. In contrast, no evident green fluorescence of A549 cells (5.24%) was found in negative control group. When the cells were treated with CDDP (5 μ M), the green fluorescence were ascendant (32.70 %), lower than that of the result of **26** (58.10 %). This phenomenon illustrated that **26** might on one hand induce tumor apoptosis by increasing production of intracellular ROS just like CDDP did. Moreover, overproduction of ROS often dissipated the mitochondrial membrane potential and led to mitochondrial dysfunction, which finally resulted in tumor death.

It was reported that DCFH-DA is not a reliable indicator for ROS measurement as many other cellular pathways can oxidize DCF-DA [54-56]. Besides, mitochondria are mainly responsible for intracellular ROS [57, 58]. Therefore, in order to give more reliable information about the ROS production in treated cells, Mito-sox was further used as probe to detect superoxide radicals in mitochondrial compartment [59]. The results in **Figure S6A1-S6C4** showed that **20**, **26** and CDDP all induced oxidative stress and **26** was the most active one in increasing the levels of ROS in mitochondria of A549 cells. In contrast, **20** could only moderately enhance the level of superoxide radicals in mitochondrial in comparison to CDDP-treated and 26-treated groups. Besides, the irregular arrangement of mitochondria in cytoplasm induced by **26** also suggested the depolarization of mitochondrial membrane potential, which was further confirmed by the following biological studies. These findings are consistent with the results from the DCFH-DA fluorescent probe. Therefore, we can clearly confirm that both **20** and **26** could increase the level of ROS in tumor cells.

*2.11. Mitochondrial Membrane Potential ($\Delta\psi_m$) depolarization induced by **26***

The generation and accumulation of ROS was closely related to the mitochondrial membrane potential ($\Delta\psi_m$), and the depolarization of mitochondrial membrane potential (MMP) was considered to be a common feature of cell death. Besides, many reports proved that Pt(IV) complexes disrupted $\Delta\psi_m$. In normal cells, mitochondria exhibit a high $\Delta\psi_m$ while in apoptotic cells $\Delta\psi_m$ dissipated [53]. Therefore, we further investigated whether $\Delta\psi_m$ was involved in the cells treated with our target compounds, using JC-1 fluorescent probe. A549 cells were co-incubated with **20** (5 μ M), **26** (5 μ M) or CDDP (5 μ M) for 24 h, stained with lipophilic cation JC-1 and analyzed with confocal laser scanning microscope evaluate $\Delta\psi_m$. As shown in **Figure 8**, after 24 h treatment with **26**, the population of cells with red fluorescence largely decreased as compared with untreated cells (**Figure 8D1-8D4**). Similarly, the $\Delta\psi_m$ of CDDP- and compound **20**-treated cells also decreased respectively (**Figure 8B1-8C4**), as reflected by decreased red fluorescence of JC-1 aggregate and the increased green fluorescence from the JC-1 monomer. The evident collapsed red fluorescence intensity indicated that $\Delta\psi_m$ has decreased sharply, suggesting that mitochondrial function changes caused by **26** were closely associated with cytotoxicity.

2.12. Cell morphology study

To explore the changes of cell morphology induced by the target compounds, A549 cells were treated with **26** (5 μ M) or **20** (5 μ M), using CDDP (5 μ M) and solvent vehicle as positive and negative control, respectively. After 24 h incubation with the tested compounds, the cells were stained with hoechst 33258 and the results were recorded with fluorescence microscope. As shown in **Figure 9A1-9D1**, A549 cells treated with 5 μ M of **26** or 5 μ M of **20** isolated from cells around, which were significantly different from that cells treated with CDDP or without treatment. Besides, there were larger population of cells treated with **26** with apoptotic nuclei containing condensed chromatin of cells whereas the cells in control culture showed regular and round outline of nuclei. To further investigate cells morphology changes, we stained A549 cells with calcein-AM/PI double staining solution after 24 h incubation of cells

with these compounds mentioned above. In **Figure 9A2-9D3**, A549 cells without drug treatment looked in spindle outline and were stained in green fluorescence, while cells became oval and irregular nucleus was observed after the treatment with CDDP, **20** and **26**, respectively. The difference of the cell morphology indicated the difference of the apoptotic inducing ability of the compounds. As was known, calcein-AM entered cells in green fluorescence, while PI could only enter apoptotic or necrotic cells and interacted with DNA in red fluorescence. Moreover, the proportion of dead cells in **20**- and **26**-treated groups (**Figure 9C3** and **9D3**) increased significantly as compared with CDDP-treated group (**Figure 9B3**), as reflected with enhanced red fluorescence from PI and the decrease of green fluorescence from calcein-AM, which indicated that both compounds were more potent in inducing apoptosis than CDDP. Therefore, characteristic color reaction also revealed that **26**-treated cells were in apoptotic status, which showed red fluorescence and differed from green fluorescence in living cells without any treatment. In conclusion, **26** exhibited better antiproliferative activity than CDDP at the same concentration after 24 h co-incubation with A549 cells.

2.13. Wound-healing assay

Metastatic cancers have several important characteristics including migration and invasion of malignant cells in the development of cancer. Therefore, we conducted a wound healing assay to detect the ability of the complex to inhibit the cell migration and invasion. A549 cells were scratched with a pipette tip and co-incubated with control (DMF), CDDP (5 μ M), **20** (1 μ M) and **26** (1 μ M) for 24 h. In order to avoid the influence of cell proliferation on the test result, the experiments were carried out under serum-starved conditions. **Figure 10** displayed the wound gaps at the time of wound generation, wound after 24 h drug-treatment, respectively. As illustrated, compound **20** and **26** significantly inhibit the wound healing at the tested concentration as compared with the negative control, whereas the CDDP-treated group obtained narrower gaps. These results indicated that both **20** and **26** could efficiently suppress A549 cells migration and further metastasis, while CDDP did not

obviously show the activity.

2.14. Western blotting study

Previous studies demonstrated that Pt(IV) complexes induced apoptosis of tumor cells by regulation of pro-/anti-apoptotic protein in a mitochondria-mediated apoptosis pathway [38], such as Bcl family proteins. Therefore, we investigated the effects of compound **26** on the expression of apoptosis-related proteins of A549 cell, using CDDP as positive control. As shown in **Figure 11A**, we could see that treatment with **26** decreased the levels of antiapoptotic protein Bcl-2 but led to the up-regulation of the proapoptotic protein Bax, indicating that **26** induced apoptosis by altering the ratio of Bcl-2 to Bax and resulting in the collapse of mitochondrial membrane potential which was previously discussed. Moreover, the elevated ratio of proapoptotic and antiapoptotic proteins promoted the release of Cyt c to cytosol, finally activating the caspase cascade and inducing tumor cell apoptosis. As shown in **Figure 11B**, when compared to control cells, caspase 9/3 were significantly activated and overexpressed in A549 cells treated with **20** or **26**, which was a critical event in the initiation and execution of apoptosis in cells. Meanwhile, the western blot data revealed that **26** also enhanced the expression of cleaved-PARP (89 KD) in comparison with untreated control. In combination with the decrease of mitochondrial membrane potential induced by **26**, we could conclude that **26** promoted apoptosis in mitochondria-mediated pathway and caspase cascade.

2.15. Antitumor Activity in Vivo

Finally, we investigated the therapeutic potential of compound **26** in A549 xenograft models to determine its antitumor efficacy in vivo. A549 cells (3×10^6) in 100 μ L of sterile PBS were injected subcutaneously in the flank of six-week-old female BALB/c athymic nude mice to establish A549 xenograft models. Thereafter, the mice were divided into four different groups (n=3) after the tumor volume reached to 150-250 mm^3 . Compounds of **20**, **26**, CDDP and saline were administered intravenously every other day for a total of 3 injections at a dose of 6 $\mu\text{mol/kg}$. The tumor volume and body weight were measured and recorded 2-3 times a week. As

shown in **Figure 12A** and **12B**, mice in control group showed a rapid increase in the average RTV (relative tumor volume) (7.1 mm^3 , **Table S1**). On the contrary, **20**, **26** and CDDP were able to suppress the growth of tumor to some extent, with IR (inhibition ratio) of 41.9%, 59.2% and 36.7%, respectively. (see **Figure 12A** and **12B**, **Table S1**). Consistent with the results of in vitro test, compound **26** showed the most potential antitumor activity in A549 xenograft mice, which may be attributed to high intracellular accumulation of **26** (**Figure 2**) and the release of CDDP (**Figure S1**). Among the tested substances, CDDP exhibited the lowest antitumor activity with RTV of 4.5 mm^3 . In addition, CDDP showed obvious side effect as reflected by the decreasing body weight, especially during days 6-12 after the first administration (**Figure 12C**). Notably, the results in **Figure 12C** strongly demonstrated that **20**, **26** did not show obvious side effects as the body weight kept increasing during the treatment. In sum, **26** did not only show significant anti-proliferative effect in vitro, but showed excellent antitumor activity in vivo, which qualified it as a 'high efficiency and low toxic' antitumor candidate.

3. Conclusion.

In conclusion, we here presented eleven novel Pt(IV) compounds conjugating with RAS/MAPK signaling disrupting agents through ester bond. Our cellular data provided evidence that most of the target Pt(IV) compounds showed higher cytotoxicity against all tested cancer lines than CDDP. Among those **26** exerted the best anti-tumor activity against A549 cells but showed only moderate cytotoxicity to normal LO2 and HUEVC cells. Moreover, **26** could overcome the multi-drug resistance and exert potent cytotoxicity to A549/CDDP and SKOV-3/CDDP cells. This unique property may be attributed to its ability to release Pt (II) complex as well as ON013100. Our stability study showed that **26** was stable in physiological environment (pH = 7.4) but was rapidly reduced and released its corresponding **20** and Pt(II) complex within 7 h under the reduction of ascorbic acid, indicating that **26** acted as a multi-functional Pt(IV) prodrug. Further biological mechanism studies indicated that **26** could efficiently disturb the signaling transduction between RAS and

MAPK pathway, by directly binding to CRAF protein. Besides, the superior cellular uptake made **26** dramatically arrest A549 cells at G2/M phase and heavily elevate apoptosis level, whereas CDDP arrested A549 cells at S phase and induced much less apoptosis. Moreover, the following mechanism studies revealed that **26** induced massive ROS, induced DNA damage, induced DNA platination and conformational changes, triggered mitochondrial membrane depolarization by inhibiting anti-apoptotic Bcl-2 and activating caspase cascade, indicating that **26** evoked apoptosis through mitochondrial apoptotic pathway. Finally, in vivo anti-tumor activities indicated that **26** efficiently inhibited tumor growth in A549 xenograft mouse model without inducing severe side effects, whereas the equimolar CDDP only gave a moderate inhibition of the tumor and caused obvious loss of body weight. The proposed antitumor action mode of **26** is outlined in **Figure 13**. Overall, we have obtained a multi-functional Pt(IV) which could inhibit the proliferation of tumor cells via two different pathways: the RAF-MEK-ERK pathway and the platinum-based cytotoxicity pathway. This unique character may qualify it as a ‘high efficiency and low toxic’ antitumor candidate.

4. Experimental section

4.1. Materials and measurements

All analytical or chemical pure reagents were obtained from commercial source unless otherwise noted. Solvents were dried over standard agents and freshly distilled prior to use. Deionized water was used in this article. The ^1H and ^{13}C NMR spectra were recorded on a Bruker Avance NMR spectrometer (300, 400 or 500 MHz for ^1H , 100 or 125 MHz for ^{13}C , 129 MHz for ^{195}Pt spectra) and chemical shifts reported (in ppm) relative to the indicated solvents. Deuterated component of CHCl_3 or $\text{DMSO-}d_6$ was used as NMR solvent. Mass spectra was obtained on an Agilent Dual ESI Q TOF 6520, in positive-ion or negative-ion model, with methanol as solvent. The thermogravimetric analysis was performed on thermogravimetry (TG 209 F3) (heating rate, 20 °C/min; starting temperature, 30 °C; finishing temperature, 800 °C; nitrogen environment). Thin-layer chromatography (TLC) was carried on glass-backed silica gel GF plates (obtained from Qingdao Marine Chemical Co., Ltd.)

and visualized by short wavelength UV light. Target compounds and intermediates were purified with silica gel (200-300 mesh) column chromatography or recrystallization. Purity of prepared compounds were determined by HPLC-UV analysis (waters, e2695 system; 2489 UV/Vis detector), using acetonitrile/water (45:55, V/V) (0.1% trifluoroacetic acid in water) as eluent except for **14** and **22** using acetonitrile/water (50:50, V/V) (0.1% trifluoroacetic acid in water) as eluent. All compounds used in biological assays were above 95%. Bax, Bcl-2, cytochrome c, cleaved-caspase-9, -3, cleaved-PARP antibodies were purchased from Imgenex, USA. Antibodies directed against p-MEK, MEK, p-ERK and ERK were purchased from Cell Signaling Technology. RAF antibody was purchased from Affinity Biosciences, whereas RAS, γ H2AX and p53 antibodies was from Abcam. Secondary antibody (1:2000) labeled with horseradish peroxidase was came from Santa Cruz Biotechnologies. TIANamp Genomic DNA Kit was purchased from TIANGEN. Mito-sox fluorescence probe was from KeyGEN BioTECH. The standard solution of platinum was from Perkin Elmer.

4.2. General methods for preparation of compounds

4.2.1. 5-formyl-2-methoxyphenyl-4-methylbenzenesulfonate (**2**)

To a solution of compound **1** (3.0 g, 19.8 mmol) in DMF (15 mL), DCM (30 mL) and Et₃N (4.0 g, 39.6 mmol), was added TsCl (4.5g, 23.8 mmol) at 0 °C and stirred at room temperature for 2 h. Progress of the reaction was monitored the reaction with TLC. After the completion of the reaction, DCM (350 mL) was added to the solution and washed with sat. NaHCO₃ (150 mL) and sat. NaCl (150 mL). The organic layer was dried with anhydrous Na₂SO₄ and concentrated under reduced pressure to get pale white solid. Purified with silica gel chromatography with the eluent of PE and EA (100:0 - 5:1, V/V) and dried at 45 °C to obtain white solid 5.8 g. Yield 95.0%; mp 143-145 °C; ¹H NMR (300 MHz, CDCl₃) δ 9.82 (s, 1H), 7.77-7.74 (m, 3H), 7.62 (d, J = 1.9 Hz, 1H), 7.32 (d, J = 8.1 Hz, 2H), 6.97 (d, J = 8.5 Hz, 1H), 3.69 (s, 3H), 2.45 (s, 3H).

4.2.2. 5-(hydroxymethyl)-2-methoxyphenyl-4-methylbenzenesulfonate (**3**)

To a solution of compound **2** (5.8 g, 18.9 mmol) in EtOH (30 mL) and DCM (15.0 mL) was added NaBH₄ (715.0 mg, 18.9 mmol) at 0 °C and stirred at room temperature for 20 min. Progress of the reaction was monitored with TLC. The reaction was worked up followed by quenching with 1 M HCl solution at 0 °C. The solvent was removed under reduced pressure and obtained crude white solid. Then DCM (300 mL) was added to dissolve the residue, washed with sat. NaCl (150 mL×3). The combined organic layer was dried with anhydrous Na₂SO₄ and concentrated in vacuum to give white solid 5.6 g. Yield 96.6%; mp 144-145 °C; ¹H NMR (300 MHz, DMSO-*d*₆) δ 7.75 (d, *J* = 8.1 Hz, 2H), 7.31 (d, *J* = 8.1 Hz, 2H), 7.24-7.20 (m, 1H), 7.14 (d, *J* = 1.9 Hz, 1H), 6.80 (d, *J* = 8.4 Hz, 1H), 4.40 (s, 2H), 3.59 (s, 3H), 2.45 (s, 3H).

4.2.3. 5-(bromomethyl)-2-methoxyphenyl-4-methylbenzenesulfonate (**4**)

To a solution of compound **3** (5.7 g, 18.5 mmol) in DCM (30 mL) at 0 °C was added slowly PBr₃ (6.0 g, 22.2 mmol) in DCM (10 mL) and stirred at the same temperature for 2 h. Progress of the reaction was monitored with TLC. After completion, the reaction was quenched with NaHCO₃ (1 M) solution at 0 °C. After that, DCM (300 mL) was added to dissolve the residue, washed with sat. NaCl (150 mL×3). The organic layer was dried with anhydrous Na₂SO₄ and concentrated in vacuum to give white solid 6.7 g. Yield 98.0%; mp 112-114 °C; ¹H NMR (300 MHz, CDCl₃) δ 7.75 (d, *J* = 8.1 Hz, 2H), 7.30 (d, *J* = 8.1 Hz, 2H), 7.23-7.20 (m, 1H), 7.14 (d, *J* = 2.0 Hz, 1H), 6.79 (d, *J* = 8.4 Hz, 1H), 4.40 (s, 2H), 3.59 (s, 3H), 2.44 (s, 3H).

4.2.4. 2-((4-methoxy-3-(tosyloxy)benzyl)thio)-acetic acid (**5**)

To a solution of compound TGA (2.2 g, 23.3 mmol) in MeOH (25 mL) at 0 °C, was added NaOH (12.0 g, 49.6 mmol) gradually and stirred for 10 min at the same temperature. Then compound **4** (5.7 g, 15.5 mmol) in 10 MeOH (25 mL) and DCM (30 mL) was dropped into the solution slowly at 0 °C. Progress of the reaction was monitored with TLC. After completion of reaction, the solvent was removed under reduced pressure to obtain pale white solid. After that, the residue was dissolved in water (70 mL), adjusted the pH to 4-5 with HCl (1 M), extracted with DCM (150

mL×3) and dried with anhydrous Na₂SO₄. The solvent was removed and concentrated under reduced pressure to obtain white solid 2.5 g. Yield 60.0%; mp 120-122 °C; ¹H NMR (400 MHz, DMSO) δ 12.64 (s, 1H), 7.68 (d, *J* = 8.2 Hz, 2H), 7.43 (d, *J* = 8.2 Hz, 2H), 7.18 (dd, *J* = 8.5, 2.1 Hz, 1H), 7.03 (d, *J* = 2.1 Hz, 1H), 6.99 (d, *J* = 8.5 Hz, 1H), 3.72 (s, 2H), 3.49 (s, 3H), 3.05 (s, 2H), 2.41 (s, 3H). HR-MS (*m/z*) (ESI) called for [C₁₇H₁₈O₆S₂-H] = 381.0545, found, 381.0561.

4.2.5. 2-((4-methoxy-3-(tosyloxy)benzyl)sulfonyl)-acetic acid (**6**)

To a solution of compound **5** (2.5 g, 6.5 mmol) in acetic acid (20 mL) at room temperature was added H₂O₂ (3.7 g, 32.7 mmol) partly and stirred at the 50 °C for 24 h. Process of the reaction was monitored with TLC. Solvent of the reaction was removed under reduced pressure to obtain pale yellow crude solid. The solid was filtered and purified with silica gel chromatography with the eluent of DCM and MeOH (100:0-50:1, V/V) to get pale white solid 1.8 g. Yield 66.7%; mp 138-140 °C; ¹H NMR (300 MHz, DMSO-*d*₆) δ 7.70 (d, *J* = 8.2 Hz, 2H), 7.43 (d, *J* = 8.2 Hz, 2H), 7.29 (dd, *J* = 8.5 Hz, 1.7 Hz, 1H), 7.19 (s, 1H), 7.09 (d, *J* = 8.5 Hz, 1H), 4.55 (s, 2H), 4.08 (s, 2H), 3.53 (s, 3H), 2.41 (s, 3H). HR-MS (*m/z*) (ESI) called for [2C₁₇H₁₈O₈S₂-H] = 827.0982, found, 827.0984.

4.2.6. (*E*)-2-methoxy-5-(((2,4,6-trimethoxystyryl)sulfonyl)methyl)phenyl-4-methylbenzenesulfonate (**8**)

To a solution of compound **6** (2.0 g, 4.8 mmol) in toluene (35 mL) at 40 °C was added piperidine (621.7 uL, 6.3 mmol) and stirred at the same temperature for 10 min. Then benzoic acid (876.4 mg, 7.2 mmol) and **7** (1.0 g, 5.3 mmol) were added to the solution slowly and heated to reflux for overnight. The reaction was monitored with TLC. After the completion of the reaction, the solution was cooled to room temperature and removed the solvent to obtain pale yellow crude product. Subsequently, the crude product was purified with silica gel chromatography with the eluent of DCM and PE (2:1, V/V) and recrystallized with DCM and PE (50 mL, 3:1, V/V) to get white solid 1.0 g. Yield 38.5%; mp 168-169 °C; ¹H NMR (300 MHz, DMSO-*d*₆) δ 7.62 (d, *J* = 8.2 Hz, 2H), 7.55 (d, *J* = 15.6 Hz, 1H), 7.35 (d, *J* = 8.2 Hz,

2H), 7.24 (d, $J = 8.4$ Hz, 1H), 7.20 (d, $J = 1.6$ Hz, 1H), 7.07 (d, $J = 15.6$ Hz, 1H), 7.02 (d, $J = 8.4$ Hz, 1H), 6.30 (s, 2H), 4.42 (s, 2H), 3.84 (s, 9H), 3.48 (s, 3H), 2.39 (s, 3H).

4.2.7. *(E)*-2,4,6-Trimethoxystyryl-3-hydroxy-4-methoxybenzylsulfone (**9**)

To a solution of compound **8** (1.0 g, 1.8 mmol) in MeOH (20 mL) and H₂O (4 mL) was added NaOH (364.6 mg, 9.1 mmol) at room temperature and stirred at 90 °C for overnight. The reaction was monitored with TLC. After the completion of the reaction, the solution was cooled to room temperature and removed the solvent to obtain pale yellow crude product. The residue was further purified with silica gel chromatography with the eluent of DCM and PE (2:1, V/V) to get pale white solid 601.0 mg. Yield 84.5%; M. p.= 128-130 °C; ¹H NMR (300 MHz, DMSO-*d*₆) δ 8.99 (s, 1H), 7.57 (d, $J = 15.6$ Hz, 1H), 7.08 (d, $J = 15.7$ Hz, 1H), 6.88 (d, $J = 8.2$ Hz, 1H), 6.80 (s, 1H), 6.73 (d, $J = 8.1$ Hz, 1H), 6.30 (s, 2H), 4.28 (s, 2H), 3.85 (s, 9H), 3.76 (s, 3H).

4.2.8. Methyl-*(E)*-2-(2-methoxy-5-(((2,4,6-trimethoxystyryl)sulfonyl)methyl)phenoxy)acetate (**10**).

To a solution of compound **9** (800.0 mg, 2.03 mmol) in DMF (15 mL) at room temperature was added slowly compound K₂CO₃ (846.9 mg, 5.07 mmol) and ethyl bromide (846.9 mg, 5.07 mmol) and stirred at 80 °C for overnight. The reaction was monitored with TLC. After completion of the reaction, the solvent was removed under reduced pressure to obtain pale yellow crude solid. The residue was dissolve in DCM (50 mL), washed with sat. NaCl (100 mL) and dried with anhydrous Na₂SO₄. The crud product was purified with silica gel chromatography with the eluent of EA/PE (5:1, V/V) and DCM/MeOH (30:1, V/V) to get pale white solid 778.07mg. Yield 80.0%; mp 104-106 °C; ¹H NMR (400 MHz, DMSO-*d*₆) δ 7.53 (d, $J = 15.7$ Hz, 1H), 7.08 (d, $J = 15.7$ Hz, 1H), 6.98 (d, $J = 8.3$ Hz, 1H), 6.93 (dd, $J = 8.3, 1.7$ Hz, 1H), 6.87 (d, $J = 1.7$ Hz, 1H), 6.30 (s, 2H), 4.61 (s, 2H), 4.35 (s, 2H), 4.13 (q, $J = 7.1$ Hz, 2H), 3.85 (d, $J = 2.2$ Hz, 9H), 3.77 (s, 3H), 1.20 (t, $J = 7.1$ Hz, 3H).

4.2.9. *(E)*-2-(2-methoxy-5-(((2,4,6-trimethoxystyryl)sulfonyl)methyl)phenoxy)-acetic acid (**11**).

To a solution of compound **10** (485.0 mg, 1.0 mmol) in EtOH (10 mL) and pure water (5 mL) at room temperature was added LiOH·H₂O (106.0 mg, 2.5 mmol) and stirred at room temperature for overnight. After the completion of the reaction, the solvent was removed under reduced pressure to obtain pale yellow solid. Added 30 mL pure water to dissolve the residue and adjusted the pH of the solution to 5 with HCl (1M). The residue was filtered and dried at 45 °C to get pale yellow solid (407.2 g, yield 90.0%); mp 112-114 °C; ¹H NMR (300 MHz, DMSO-*d*₆) δ 12.88 (s, 1H), 7.54 (d, *J* = 15.7 Hz, 1H), 7.09 (d, *J* = 15.7 Hz, 1H), 6.97 (d, *J* = 8.1 Hz, 1H), 6.91 (d, *J* = 8.1 Hz, 1H), 6.89 (s, 1H), 6.29 (s, 2H), 4.51 (s, 2H), 4.34 (s, 2H), 3.85 (s, 9H), 3.77 (s, 3H). HR-MS (*m/z*) (ESI) called for [C₂₁H₂₄O₉S-H] = 451.1163, found, 451.1170.

4.2.10. General procedure for preparing compounds **12-14**

To a solution of compound **11** (148 mg, 0.33 mmol) in DMF (3 mL) was added compound TBTU (158.9 mg, 0.50 mmol) and stirred at room temperature for 5 min. Then, Et₃N (68.0 uL, 0.50 mmol) was added to the solution under the protection of nitrogen and stirred for 5min at the same temperature. After that, compound **15, 16, 17** (0.36 mmol) was added to the solution under the protection of nitrogen and stirred for 2 h at 35 °C. Progress of the reaction was monitored with TLC. After the completion of the reaction, DCM (250 mL) was added to the solution and washed with sat. NaCl (100 mL). The organic layer was dried with anhydrous Na₂SO₄ and concentrated under reduced pressure to obtain crude product. DCM (50 mL) was added to dissolve the residue and purified with silica gel chromatography with the eluent of DCM and MeOH (60:1-20:1, V/V) to get target compounds.

4.2.11. (*OC-6-33*)-diamminetrichlorido((*E*)-2-(2-methoxy-5-(((2,4,6-trimethoxystyryl)sulfonyl)methyl)phenoxy)acetate)-platinum(IV) (**12**). Pale yellow solid. Yield: 30.1%; mp (decomp.) 169-172 °C; ¹H NMR (300 MHz, DMSO-*d*₆) δ 7.54 (d, *J* = 15.7 Hz, 1H), 7.09 (d, *J* = 15.7 Hz, 1H), 6.94 (d, *J* = 8.2 Hz, 1H), 6.93 (s, 1H), 6.88 (d, *J* = 8.2 Hz, 1H), 6.25 (m, 8H), 4.50 (s, 2H), 4.33 (s, 2H), 3.86 (s, 9H), 3.76 (s, 3H); ¹³C NMR (75 MHz, DMSO-*d*₆) δ 175.74, 164.40, 161.72 (2×Ar-OCH₃, overlapped signals),

149.34, 147.35, 133.81, 124.31, 123.62, 121.56, 116.94, 112.24, 102.89, 91.40 (2×Ar-H, overlapped signals), 65.98, 60.37, 60.29(2×CH₃O-, overlapped signals), 56.64, 56.00. ¹⁹⁵Pt NMR (129 MHz, DMSO-*d*₆): δ/ppm 551.96; HR-MS (*m/z*) (ESI): called for [C₂₁H₂₉Cl₃N₂O₉PtS-H] = 785.0214, found, 785.0334.

4.2.12. (OC-6-34)-chlorido(dicarboxylate)(cyclohexane-1*R*,2*R*-diamine)((*E*)-2-(2-methoxy-5-(((2,4,6-trimethoxystyryl)sulfonyl)methyl)phenoxy)acetate)-platinum(IV) (**13**). Pale yellow solid. Yield: 60.2%; mp (decomp.) 178-180 °C; ¹H NMR (500 MHz, DMSO-*d*₆) δ 8.35 (s, 1H), 8.26 (s, 1H), 8.03 (s, 1H), 7.64 (s, 1H), 7.55 (d, *J* = 15.7 Hz, 1H), 7.10 (d, *J* = 15.7 Hz, 1H), 6.96 (d, *J* = 8.3 Hz, 1H), 6.90 (d, *J* = 8.3 Hz, 1H), 6.82 (s, 1H), 6.30 (s, 2H), 4.55 (s, 2H), 4.34 (s, 2H), 3.85 (s, 9H), 3.76 (s, 3H), 2.56 (s, 1H), 2.49 – 2.43 (m, 1H), 2.02 (m, 2H), 1.52 (m, 1H), 1.45 (m, 2H), 1.31 (m, 1H), 1.18 – 0.95 (m, 2H); ¹³C NMR (125 MHz, DMSO-*d*₆) δ 175.52, 164.15, 163.71(2×-COO-, overlapped signals), 161.41(2×Ar-OCH₃, overlapped signals), 149.38, 147.25, 133.55, 124.65, 123.74, 121.55, 116.31, 112.45, 103.09, 91.43 (2×Ar-H, overlapped signals), 66.59, 62.01, 61.59, 60.02, 56.54 (2×CH₃O-, overlapped signals), 56.10, 56.06, 31.38, 30.94, 23.99, 23.88. ¹⁹⁵Pt NMR (129 MHz, DMSO-*d*₆): δ/ppm 995.55; HR-MS (*m/z*) (ESI): [C₂₉H₃₇ClN₂O₁₃PtS-H] = 883.1377, found 883.1385.

4.2.13. (OC-6-33)-trichlorido(cyclohexane-1*R*,2*R*-diamine)((*E*)-2-(2-methoxy-5-(((2,4,6-trimethoxystyryl)sulfonyl)methyl)phenoxy)acetate)-platinum(IV) (**14**). Pale yellow solid. Yield: 30.0%; mp (decomp.) 176-178 °C; ¹H NMR (500 MHz, DMSO-*d*₆) δ 9.08 (s, 1H), 8.16 (s, 1H), 7.88 (s, 1H), 7.53 (d, *J* = 15.7 Hz, 2H), 7.09 (d, *J* = 15.6 Hz, 1H), 6.95 (d, *J* = 8.3 Hz, 1H), 6.90 (d, *J* = 8.3 Hz, 1H), 6.86 (s, 1H), 6.29 (s, 2H), 4.54 (s, 2H), 4.32 (q, *J* = 13.6 Hz, 2H), 3.86 (s, 9H), 3.76 (s, 3H), 2.75 (s, 1H), 2.15 (m, 1H), 2.06 (m, 1H), 1.54 (m, 1H), 1.46 (m, 2H), 1.24 (m, 2H), 1.03 (m, 2H); ¹³C NMR (75 MHz, DMSO) δ 178.01, 164.15, 161.40 (2×Ar-OCH₃, overlapped signals), 149.32, 147.16, 133.64, 124.48, 123.69, 121.58, 116.59, 112.40, 102.99, 91.45 (2×Ar-H, overlapped signals), 66.82, 63.89, 62.90, 60.24, 56.62 (2×CH₃O-, overlapped signals), 56.10, 56.05, 31.41, 31.29, 23.93 (2×-CH₂CH₂-, overlapped signals). ¹⁹⁵Pt NMR (129

MHz, DMSO $-d_6$): δ /ppm 404.15; HR-MS (m/z) (ESI) called for $[C_{27}H_{37}Cl_3N_2O_9PtS-H] = 865.0943$, found 865.0967.

4.1.14. General procedure for preparing compounds **19,20**

To a solution of compound **9** (500.0 mg, 1.27 mmol) in DMF (10 mL) was added K_2CO_3 (692.0 mg, 5.07 mmol) and stirred at room temperature for 5 min. Then, succinic anhydride (5.07 mmol) or slutaric anhydride (5.07 mmol) was added to the solution under the protection of nitrogen and stirred for 30 min at 50 °C. Progress of the reaction was monitored with TLC. After the completion of the reaction, the solvent of the reaction was removed under reduced pressure. After that, water (100 mL) was added to dissolve the residue, adjusted the pH to 4-5 and extracted with DCM (50 mL \times 3). The combined organic layer was washed with sat. NaCl (100 mL), dried with anhydrous Na_2SO_4 , concentrated under reduced pressure to obtain crude product. Finally, the crud product was further purified by silica gel chromatography with the eluent of DCM and MeOH (100:1-60:1) to get white solid.

4.2.15. (*E*)-4-(2-methoxy-5-(((2,4,6-trimethoxystyryl)sulfonyl)methyl)phenoxy)-4-oxobutanoic acid (**19**). White solid. Yield: 31.0%; mp 155-157 °C; 1H NMR (600 MHz, DMSO) δ 12.31 (s, 1H), 7.58 (d, $J = 15.6$ Hz, 1H), 7.21 (dd, $J = 8.5$ Hz, 2.1 Hz, 1H), 7.11 (d, $J = 8.5$ Hz, 1H), 7.08 (d, $J = 15.6$ Hz, 1H), 7.06 (d, $J = 2.1$ Hz, 1H), 6.29 (s, 2H), 4.41 (s, 2H), 3.85-3.75 (m, 9H), 3.75 (s, 3H), 2.79-2.76 (m, 2H), 2.57 – 2.55 (m, 2H). HR-MS (m/z) (ESI): $[C_{23}H_{26}O_{10}S-C_4H_5O_3] = 393.1008$, found 393.1189.

4.2.16. (*E*)-5-(2-methoxy-5-(((2,4,6-trimethoxystyryl)sulfonyl)methyl)phenoxy)-5-oxopentanoic acid (**20**). White solid. Yield 75.2%; mp 152-154 °C; 1H NMR (400 MHz, DMSO- d_6) δ 12.18 (s, 1H), 7.58 (d, $J = 15.6$ Hz, 1H), 7.22 (dd, $J = 8.5$, 2.0 Hz, 1H), 7.12 (d, $J = 8.5$ Hz, 1H), 7.09 (d, $J = 15.6$ Hz, 1H), 7.08 (d, $J = 2.0$ Hz, 1H), 6.30 (s, 2H), 4.42 (s, 2H), 3.85-3.86 (m, 9H), 3.77 (s, 3H), 2.60 (t, $J = 7.4$ Hz, 2H), 2.35 (t, $J = 7.4$ Hz, 2H), 1.87-1.80 (m, 2H). HR-MS (m/z) (ESI) called for $[2C_{24}H_{28}O_{10}S-H] = 1015.2650$, found 1015.2913.

4.2.17. (*OC*-6-33)-trichlorido(cyclohexane-1*R*,2*R*-diamine)((*E*)-4-(2-methoxy-5-(((2,4,6-trimethoxystyryl)sulfonyl)methyl)phenoxy)-4-oxobutanoicate)-platinum(IV) (**21**).

Yield: 49.0%. Pale yellow solid; mp (decomp.) 180-184 °C; ^1H NMR (400 MHz, DMSO) δ 9.43 (s, 1H), 8.06 (s, 1H), 7.86 (s, 1H), 7.58 (d, $J = 15.6$ Hz, 1H), 7.42 (s, 1H), 7.21 (d, $J = 7.4$ Hz, 1H), 7.13-7.07 (m, 3H), 6.30 (s, 2H), 4.39 (s, 2H), 3.86 (s, 9H), 3.76 (s, 3H), 2.73 (s, 1H), 2.69 (s, 2H), 2.63 (s, 2H), 2.16-2.14 (m, 1H), 2.01-1.98 (m, 1H), 1.54 – 1.34 (m, 3H), 1.26-1.01 (m, 3H), 0.91-0.82 (m, 1H); ^{13}C NMR (100 MHz, DMSO- d_6) δ 181.54, 170.96, 164.19, 161.44 ($2\times\text{Ar-OCH}_3$, overlapped signals), 151.39, 139.34, 133.76, 130.12, 125.74, 123.68, 121.83, 113.01, 103.02, 91.44 ($2\times\text{Ar-H}$, overlapped signals), 63.51, 62.62, 59.61, 56.57 ($2\times\text{CH}_3\text{O-}$, overlapped signals), 56.39, 56.13, 32.38, 32.34, 31.31, 29.89, 24.05, 23.75. ^{195}Pt NMR (129 MHz, DMSO- d_6): δ/ppm 418.66; HR-MS (m/z) (ESI) called for [$\text{C}_{29}\text{H}_{39}\text{Cl}_3\text{N}_2\text{O}_{10}\text{PtS} + \text{H}$] = 909.2290, found 909.2282.

4.2.18. (OC-6-33)-trichlorido(cyclohexane-1R,2R-diamine)((E)-5-(2-methoxy-5-(((2,4,6-trimethoxystyryl)sulfonyl)methyl)phenoxy)-5-oxopentanoate)-platinum(IV) (**22**).

Yield: 51.0%. Pale yellow solid; mp (decomp.) 153 -155 °C; ^1H NMR (400 MHz, DMSO- d_6) δ 9.58 (s, 1H), 8.18 (s, 1H), 7.84 (s, 1H), 7.57 (d, $J = 15.6$ Hz, 1H), 7.53 – 7.42 (m, 1H), 7.22 (d, $J = 8.1$ Hz, 1H), 7.14 – 7.05 (m, 3H), 6.30 (s, 2H), 4.42 (s, 2H), 3.86 (s, 9H), 3.77 (s, 3H), 2.76-2.72 (m, 1H), 2.62 (t, $J = 6.6$ Hz, 2H), 2.39 (d, $J = 2.2$ Hz, 2H), 2.21 – 2.15 (m, 1H), 2.08-2.05 (m, 1H), 1.88 – 1.80 (m, 2H), 1.56 – 1.45 (m, 3H), 1.33 – 1.25 (m, 1H), 1.11-1.02 (m, , 3H); ^{13}C NMR (100 MHz, DMSO- d_6) δ 182.92, 171.24, 164.19, 161.44 ($2\times\text{Ar-OCH}_3$, overlapped signals), 151.32, 139.35, 133.77, 130.13, 125.67, 123.66, 121.95, 113.01, 103.02, 91.44 ($2\times\text{Ar-H}$, overlapped signals), 63.90, 62.72, 59.60, 56.58 ($2\times\text{CH}_3\text{O-}$, overlapped signals), 56.39, 56.14, 38.72, 36.69, 32.87, 31.40, 31.33, 24.04, 21.46. ^{195}Pt NMR (129 MHz, DMSO- d_6): δ/ppm 417.02; HR-MS (m/z) (ESI) called for [$\text{C}_{30}\text{H}_{41}\text{Cl}_3\text{N}_2\text{O}_{10}\text{PtS-H}$] = 921.1106, found 921.1192.

4.2.19. (OC-6-34)-chlorido(dicarboxylate)(cyclohexane-1R,2R-diamine)((E)-4-(2-methoxy-5-(((2,4,6-trimethoxystyryl)sulfonyl)methyl)phenoxy)-4-oxobutanoate)-platinum(IV) (**23**). Yield: 61.0%. Pale yellow solid; mp (decomp.) 176 -178 °C; ^1H NMR (400 MHz, DMSO- d_6) δ 8.39-8.37 (m, 1H), 8.29 – 8.24 (m, 2H), 7.66-7.64 (m, 1H),

7.57 (d, $J = 15.6$ Hz, 1H), 7.21 (d, $J = 8.5$ Hz, 1H), 7.12 – 7.10 (m, 2H), 7.08 – 7.07 (m, 1H), 6.30 (s, 2H), 4.40 (s, 2H), 3.85 (s, 9H), 3.75 (s, 3H), 2.77-2.72 (m, 2H), 2.67-2.66 (m, 2H), 2.07 (d, $J = 11.3$ Hz, 1H), 1.96 (d, $J = 10.7$ Hz, 1H), 1.56 – 1.50 (m, 1H), 1.43-1.28 (m, 3H), 1.33-1.30 (m, 2H), 1.00-0.86 (m, 2H); ^{13}C NMR (100 MHz, DMSO- d_6) δ 179.37, 170.98, 164.19, 163.74, 163.69, 161.44 ($2\times\text{Ar-OCH}_3$, overlapped signals), 151.35, 139.31, 133.72, 130.12, 125.76, 123.71, 121.89, 113.01, 103.03, 91.45 ($2\times\text{Ar-H}$, overlapped signals), 61.90, 61.62, 59.58, 56.55 ($2\times\text{CH}_3\text{O-}$, overlapped signals), 56.38, 56.11, 31.61, 31.32, 31.03, 29.74, 23.99, 23.81. ^{195}Pt NMR (129 MHz, DMSO- d_6): δ /ppm 1001.05; HR-MS (m/z) (ESI) called for $[\text{C}_{31}\text{H}_{39}\text{ClN}_2\text{O}_{14}\text{PtS+H}] = 927.2550$, found 927.2759.

4.2.20. (OC-6-34)-chlorido(dicarboxylate)(cyclohexane-1R,2R-diamine)((E)-5-(2-methoxy-5-(((2,4,6-trimethoxystyryl)sulfonyl)methyl)phenoxy)-5-oxopentanoate)-platinum(IV) (**24**). Yield: 50.9%. Pale yellow solid; mp (decomp.) 173 -175 °C; ^1H NMR (400 MHz, DMSO- d_6) δ 8.40-8.35 (m, 3H), 7.68-7.66 (m, 1H), 7.58 (d, $J = 15.6$ Hz, 1H), 7.21 (dd, $J = 8.5, 1.8$ Hz, 1H), 7.13 – 7.06 (m, 3H), 6.30 (s, 2H), 4.41 (s, 2H), 3.85 (s, 9H), 3.75 (s, 3H), 2.59-2.56 (m, 4H), 2.42 (t, $J = 7.4$ Hz, 2H), 2.11-2.01 (m, 2H), 1.83-1.80 (m, 2H), 1.56-1.46 (m, 4H), 1.18-1.06 (m, 2H); ^{13}C NMR (100 MHz, DMSO- d_6) δ 180.43, 171.17, 164.19, 163.72 ($2\times\text{-COO-}$, overlapped signals), 161.44 ($2\times\text{Ar-OCH}_3$, overlapped signals), 151.31, 139.32, 133.77, 130.15, 125.64, 123.66, 121.94, 112.99, 103.01, 91.44 ($2\times\text{Ar-H}$, overlapped signals), 61.99, 61.85, 59.58, 56.55 ($2\times\text{CH}_3\text{O-}$, overlapped signals), 56.33, 56.12, 35.84, 32.90, 31.37, 31.05, 24.00 ($2\times\text{-CH}_2\text{CH}_2\text{-}$, overlapped signals), 21.27. ^{195}Pt NMR (129 MHz, DMSO- d_6): δ /ppm 1001.30; HR-MS (m/z) (ESI) called for $[\text{C}_{32}\text{H}_{41}\text{ClN}_2\text{O}_{14}\text{PtS-H}] = 939.1615$, found 939.1629.

4.2.21. (OC-6-33)-diamminetrichlorido((E)-4-(2-methoxy-5-(((2,4,6-trimethoxystyryl)sulfonyl)methyl)phenoxy)-4-oxobutanoate))-platinum(IV) (**25**). Yield: 45.1%, Pale yellow solid; mp (decomp.) 170 -172 °C; ^1H NMR (400 MHz, DMSO- d_6) δ 7.57 (d, $J = 15.6$ Hz, 1H), 7.22-7.20 (m, 1H), 7.12- 7.07 (m, 3H), 6.40 – 6.05 (m, 8H), 4.41 (s, 2H), 3.86-3.85 (m, 9H), 3.76 (s, 3H), 2.74 (t, $J = 7.2$ Hz, 2H), 2.62 (t, $J = 7.2$ Hz,

2H); ^{13}C NMR (100 MHz, $\text{DMSO-}d_6$) δ 179.10, 170.92, 164.19, 161.44 ($2\times\text{Ar-OCH}_3$, overlapped signals), 151.34, 139.36, 133.76, 130.10, 125.78, 123.68, 121.86, 113.02, 103.01, 91.44 ($2\times\text{Ar-H}$, overlapped signals), 59.61, 56.58 ($2\times\text{CH}_3\text{O-}$, overlapped signals), 56.40, 56.15, 31.44, 30.10. ^{195}Pt NMR (129 MHz, $\text{DMSO-}d_6$): δ/ppm 531.92; HR-MS (m/z) (ESI) called for $[\text{C}_{23}\text{H}_{31}\text{Cl}_3\text{N}_2\text{O}_{10}\text{PtS}+\text{H}] = 829.0466$, found 829.1240.

4.2.22. (OC-6-33)-diamminetrichlorido((E)-5-(2-methoxy-5-(((2,4,6-trimethoxystyryl)sulfonyl)methyl)phenoxy)-5-oxopentanoicate)-platinum(IV) (**26**). Yield: 50.7%. Pale yellow solid; mp (decomp.) 169 -171 °C; ^1H NMR (400 MHz, $\text{DMSO-}d_6$) δ 7.58 (d, $J = 15.3$ Hz, 1H), 7.21 (s, 1H), 7.10-1.07 (m, 3H), 6.30-6.20 (m, 8H), 4.41 (s, 2H), 3.86-3.77 (m, 12H), 2.63 (br. s, 2H), 2.37 (br. s, 2H), 1.82 (br. s, 2H); ^{13}C NMR (100 MHz, $\text{DMSO-}d_6$) δ 180.17, 171.42, 164.18, 161.44 ($2\times\text{Ar-OCH}_3$, overlapped signals), 151.34, 139.35, 133.77, 130.12, 125.68, 123.66, 121.93, 113.00, 103.02, 91.45 ($2\times\text{Ar-H}$, overlapped signals), 59.58, 56.59 ($2\times\text{CH}_3\text{O-}$, overlapped signals), 56.39, 56.16, 35.49, 32.99, 21.42. ^{195}Pt NMR (129 MHz, $\text{DMSO-}d_6$): δ/ppm 529.87; HR-MS (m/z) (ESI) called for $[\text{C}_{24}\text{H}_{33}\text{Cl}_3\text{N}_2\text{O}_{10}\text{PtS}-\text{H}] = 841.0578$, found 841.0570.

4.2.23. (OC-6-33)-dichlorido(hydroxyl)((E)-4-(2-methoxy-5-(((2,4,6-trimethoxystyryl)sulfonyl)methyl)phenoxy)-4-oxobutanoicate))-platinum(IV) (**27**). Yield: 35.1%. Pale yellow solid; mp (decomp.) 168 -170 °C; ^1H NMR (400 MHz, $\text{DMSO-}d_6$) δ 7.58 (d, $J = 15.6$ Hz, 1H), 7.21 (dd, $J = 8.5, 2.0$ Hz, 1H), 7.14 – 7.06 (m, 3H), 6.30 (s, 2H), 6.09-5.83 (m, 6H), 4.41 (s, 2H), 3.86=3.85 (m, 9H), 3.77 (s, 3H), 2.72 (t, $J = 7.2$ Hz, 2H), 2.55 (d, $J = 7.2$ Hz, 2H); ^{13}C NMR (100 MHz, $\text{DMSO-}d_6$) δ 179.53, 171.11, 164.18, 161.43 ($2\times\text{Ar-OCH}_3$, overlapped signals), 151.35, 139.39, 133.74, 130.06, 125.80, 123.67, 121.84, 113.00, 103.00, 91.44 ($2\times\text{Ar-H}$, overlapped signals), 59.60, 56.58 ($2\times\text{CH}_3\text{O-}$, overlapped signals), 56.39, 56.14, 31.59, 30.27. ^{195}Pt NMR (129 MHz, $\text{DMSO-}d_6$): δ/ppm 1221.32; HR-MS (m/z) (ESI) called for $[\text{C}_{23}\text{H}_{32}\text{Cl}_2\text{N}_2\text{O}_{11}\text{PtS}+\text{H}] = 811.0811$, found 811.0964.

4.2.24. (OC-6-33)-dichlorido(hydroxyl)((E)-4-(2-methoxy-5-(((2,4,6-trimethoxystyryl)sulfonyl)methyl)phenoxy)-5-oxopentanoicate))-platinum(IV) (**28**). Yield: 38.1%. Pale yellow solid; mp (decomp.) 175 -177 °C; ^1H NMR (400 MHz, $\text{DMSO-}d_6$) δ 7.57 (d, J

= 15.6 Hz, 1H), 7.22-7.20 (m, 1H), 7.15 – 7.04 (m, 3H), 6.28 (s, 2H), 6.18 – 5.81 (m, 6H), 4.41 (s, 2H), 3.86-3.77 (m, 13H), 2.60 (t, $J = 6.8$ Hz, 2H), 2.30 (t, $J = 6.8$ Hz, 2H), 1.87 – 1.76 (m, 2H); ^{13}C NMR (100 MHz, DMSO- d_6) δ 180.67, 171.46, 164.18, 161.44 ($2 \times \text{Ar-OCH}_3$, overlapped signals), 151.35, 139.36, 133.76, 130.10, 125.68, 123.66, 121.93, 113.00, 102.97, 91.19 ($2 \times \text{Ar-H}$, overlapped signals), 59.58, 56.59 ($2 \times \text{CH}_3\text{O-}$, overlapped signals), 56.38, 56.15, 35.63, 33.11, 21.59. ^{195}Pt NMR (129 MHz, DMSO- d_6): δ /ppm 1228.16; HR-MS (m/z) (ESI) called for $[\text{C}_{24}\text{H}_{34}\text{Cl}_2\text{N}_2\text{O}_{11}\text{PtS-H}] = 823.0823$, found 823.0905.

4.3. Cell culture

Adherent cells used in this article, including A549 cells (non-small cell lung cancer cell line), OVCaR-3 (ovarian cancer cell line), SGC-7901 cells (gastric cancer cell line), HCT-116 cells (human colon cancer cell), A549/CDDP cells (cisplatin-resistant non-small cell lung cancer cell line) were maintained in exponential growth in RPMI 1640 medium (Life Technologies Gibco) supplemented with 10 % fetal bovine serum, penicillin (100 $\mu\text{g/mL}$) and streptomycin (100 $\mu\text{g/mL}$) solution. The OVCaR-3 cells (ovarian cancer cell line), SKOV-3/CDDP cells (cisplatin-resistant ovarian cancer cell line) HUEVC cells (human endothelial vein cells) and LO2 cells (human normal liver cell line) were cultured in Dulbecco's Modified Eagle's Medium (DMEM) (Life Technologies Gibco) supplemented with 10 % fetal bovine serum, penicillin (100 $\mu\text{g/mL}$) and streptomycin (100 $\mu\text{g/mL}$) solution. All cells were grown monolayer in a humidified atmosphere of 5 % CO_2 and 95 % air at 37.0 $^\circ\text{C}$. Besides, the SKOV-3/CDDP cells and A549/CDDP cells were constructed following the methods reported previously [60, 61]. Briefly, A549 or SKOV-3 cancer cells were exposed to CDDP at the initial concentration of 3 nM three times for 3-day period in the following two months. Thereafter, the concentration of CDDP was double and repeated the procedure until the final concentration of 40 μM was achieved for more than 90 % percentage of cell viability.

4.4. Cytotoxicity Assay

The MTT method was used to determine the cytotoxicity in vitro of test

compounds against A549 cells, OVCaR-3 cells, SGC-7901 cells, HCT-116 cells, A549/CDDP cells, SKOV-3/CDDP cells, HUVEC cells and LO2 cells. Freshly trypsinized cells suspensions with a density of 3.0×10^4 cells/well were seeded in 96-well microtiter plates and incubated in atmosphere of 5% CO₂ and 95% air at 37.0 °C for overnight. Then, test compounds dissolved in DMF and diluted to various concentrations with medium were added respectively to those cells mentioned above. After 72 h treatment, the incubation was worked up by addition of 20 μL MTT (5 mg/mL) and those cells were incubated for another 4 h at the same condition. Then the supernatant fraction of each well was abandoned, 150 μL DMSO was added and mixed fully with each other on shaking table. The O.D. value of each well was read with enzyme labelling instrument at 490 nm. Finally, the IC₅₀ value of each compound was calculated with SPSS software with three parallel experiments.

4.5. HPLC analysis of activation of **26** by reduction

The release of compound **20** and stability of compound **26** in different environments were detected using a reverse-phase high performance liquid phase chromatography (waters, e2695 system; 2489 UV/Vis detector). The stability of compound **26** was performed in a solution of **26** (2.0 mg, 0.5 mM) in PBS (pH= 7.4) and acetonitrile (5 mL, 90:10, V/V). A mixture of compound **26** (2.0 mg, 0.5 mM) and ascorbic acid (1.3 mg, 1.5 mM) in PBS (pH= 7.4) and acetonitrile (5 mL, 90:10, V/V) was used to investigate its stability. All solutions prepared were preserved at 37 °C water bath in dark, detected and recorded by RP-HPLC on ODS column (250×4.6 mm, 5 μm) at different time points with eluent of acetonitrile/water (45:55, V/V) (0.1% trifluoroacetic acid in water). Similarly, ascorbic acid and **20** were dissolved respectively in the same solution as control to match the peaks appeared in the reduction process of **26**. The flow rate was 1.0 mL/min and the volume of sample injection was more than 20.0 μL. All of the compounds tested with RP-HPLC were purified with 0.45μm filter. The wavelength for testing was 254 nm. As for CDDP detection, A549 cells were incubated with **26** for 24 h followed by lysis and filtration with millipore filtration (0.22 μm). The results were recorded and annualized with

HR-MS instrument.

4.6. Cell uptake assay and DNA platination assay

A549 cells were grown in 96-well plates in grow medium until the cells reached about 80% confluence. Then the cells were treated with CDDP (5 μ M, 10 μ M), **26** (5 μ M, 10 μ M), respectively, for 12 h. After treatment with various conditions, the cells were collected and washed with ice cold PBS (3 \times 3 mL), centrifuged at 1000 \times g and resuspended in PBS (1 mL). The cell density was obtained using 100 μ L suspension, and the rest cells were measured the platinum content by ICP-MS after digestion with 65% HNO₃ (200 μ L).

In order to investigate the platinum content binding to DNA, the DNA platinum in A549 cells was studied. Therefore, A549 cells were grown in 6-well plates at a density of 50×10^3 cell/well and incubated with CDDP (2.5 μ M, 5 μ M, 10 μ M) and **26** (2.5 μ M, 5 μ M, 10 μ M) after 80% confluence of cells. After 12 h co-incubation, the free drugs in the medium was washed with cold PBS buffer and the cells were harvested, centrifuged (4400 rpm, 5 min) and resuspended in PBS (1 mL). The platinum DNA in A549 cells was isolated with TIANamp Genomic DNA kit (TIANGEN) under the instructions of the manufacturer and determined with NanoDrop 2000 (Thermo Scientific). Finally, the remaining DNA solutions were digested with 65% HNO₃, analyzed and recorded with ICP-MS. The results were presented with ng/ μ g of Pt/DNA.

4.7. Gel electrophoretic assays

In order to directly investigate the effect made by CDDP, **20** and **26** on DNA, various concentrations of CDDP (1.25, 2.5, 5, 10, 20 and 40 μ M), **26** (1.25, 2.5, 5, 10, 20 and 40 μ M) which was pre-treated with ascorbic acid (3.0 equiv.) at 37 °C in dark were used as test groups and **20** (2.5, 5, 10, 20 and 40 μ M), **26** (2.5, 5, 10, 20 and 40 μ M) were used as controls. Similarly, pBR322 plasmid DNA was used as target. Compounds **20** and **26** were dissolved in DMF and diluted to desired concentrations, whereas incubated **26** was obtained by 7 h co-incubation with ascorbic acid (3.0 equiv.) at 37 °C in dark. Firstly, pBR322 plasmid DNA was co-incubated with

various concentrations of those test compounds for 3 h at 37 °C in dark, followed with performing gel electrophoresis of 1 % agarose gel in TA buffer (50 mM Tris-acetate, pH 7.5) at 80 V for 2 h. Bands of pBR322 plasmid DNA, which were stained with ethidium bromide, were recorded and analysed with Molecular Imager (Bio-Rad, USA) under UV light.

4.8. Co-immunoprecipitation assay

In order to determine the effect of **26** interrupting the signaling transduction between RAS and RAF, co-immunoprecipitation assay was performed. A549 cells were cultured and treated with same concentration **20** and **26**, respectively, following the method mentioned in method 4.10. After co-incubation with **20** and **26** for 24h, A549 cells were collected, washed with cold PBS and digested with trypsin at 37 °C. Lysates obtained from A549 cells lysed in lysis buffer at 4 °C were incubated with VE-cadherin (contained primary antibody) at 4 °C for overnight. Subsequently, the immune complexes were precipitated with protein G agarose, centrifuged, washed with cold PBS and resolved with SDS-PAGE. The final proteins were subjected to western blot analysis, using the antibody mentioned above.

4.9. Microscale Thermophoresis (MST) assay

To determine the binding constant (Kd), microscale thermophoresis (MST) assay was performed, using CRAF RBD protein (aa 1-149, EMD Millipore) and KRAS protein (Sino Biological Inc.). Firstly, KRAS protein was N-terminally labeled using the Monolith NT Protein Labeling Kit RED-NHS (NanoTemper Technologies, München, Germany), following the illustrations of manufacturer. And the CRAF was labeled with FITC by FITC-OSu in PBS (pH=7.4) solution and the protein eluted in 0.5 mL of binding buffer (25 mM Tris-HCl, pH 8.0/ 300mM NaCl) [15, 62].

Subsequently, the Kd results of CRAF RBD protein or KRAS protein and **26** were recorded with the Monolith NT.115 (Nano Temper Technologies) and analysed with MO affinity analysis software, using the concentration 100 nM of proteins and **20** (25 µM to 0.000763 nM), **26** (25 µM to 0.000763 nM) or **26** (62.5 µM to 0.00381 nM). The assays were carried out 16-point serial dilution after 30 min co-incubation

in dark at room temperature, using binding buffer of (25mM Tris-HCl, pH 8.0/300 mM NaCl) or (40 mM HEPES, pH 7.5, 5 mM MgCl₂, 100 mM NaCl, plus 0.05% TWEEN-20, and 2–4% DMSO). The measurements were done using 20% LED and 40% MST power at room temperature.

4.10. Cellular thermal shift assay

In order to determine the effect of CRAF protein induced by **26** cellular thermal shift assay was carried out. Firstly, the A549 cell lysates were separated into three aliquots and co-incubated with various compounds of **20** (5 μM), **26** (5 μM) and DMF for 30 min at room temperature. Thereafter, the lysates of each group was divided into 20 μL into 6 PCR tubes and heated to different temperature ranging from 47 °C to 67 °C for 5 min, centrifuged and the supernatants were subjected to western blotting, using anti-KRAS and anti-CRAF antibodies. The results were analysed with image J software.

4.11. Apoptosis analysis

Freshly trypsinized non-small cell lung cancer (A549) suspensions with a density of 3.0×10^4 cells/well were seeded in 96-well microtiter plates and incubated in atmosphere of 5% CO₂ and 95% air at 37.0 °C for overnight. Then, cisplatin (5 μM), compound **20** (2 μM and 5 μM), **26** (2 μM and 5 μM) dissolved in DMF were added respectively to the medium and incubated for 24 h at the same condition. Then, the cells were washed with ice PBS after the collection of medium, trypsinized and centrifuged. After that, the cells were resuspended with 195 μL Annexin V-FITC Binding Buffer, treated with 5μL Annexin V-FITC (BD, Pharmingen) and 5 μL propidium iodide (PI) and incubated at room temperature in dark for 10 min. The apoptosis value was obtained with system software (Cell Quest; BD Biosciences).

4.12. Cell cycle arrestment assay

A549 cells were plated in 6-well cell plate in the RPMI 1640 medium with 10% FBS and allowed to adhere overnight. After incubation overnight, the tumor cells were treated with different compounds: compound **20** (5 μM), compound **26** (5 μM), CDDP (5 μM), and vehicle (DMF) for 24 h. The cells were trypsinized and pelleted.

Then, the cells were collected and washed twice with ice-cold PBS and fixed with ice-cold ethanol at -20 °C overnight. After that, the cells were washed twice with cold PBS and treated with RNase A (100 µg/mL) at 37 °C for 20 min, centrifuged and collected. The cells were then stained with propidium iodide (1mg/mL) in dark at 4 °C for 30 min following the instructions of test kit, and analyzed with system software (Cell Quest; BD Biosciences).

4.13. Comet assay

A549 cells were plated in 6-well cell plate in the RPMI 1640 medium with 10% FBS and allowed to adhere overnight. Thereafter, the cells were co-incubated with various compounds of **20** (5 µM), **26** (5 µM), CDDP (5 µM), and vehicle (DMF) for 24 h. Then the cells were washed with fresh PBS and 10 µL of cell suspension was mixed with 100 µL 1% low temperature agarose. The mixture was dropped onto glass slides and placed with glass coverslips, allowing to fixed at 4 °C for 10 min. Then, the cells were lysed at 4 °C for 1 h and immersed in lysis buffer for 30 min at 4 °C before incubated in alkaline unwinding solution (1 mM EDTA, 200 mM NaOH) for 20 min at room temperature. After electrophoresis, the slides were stained with pyridinium iodide at 4 °C for 10 min in darkness and covered with coverslips. The results were recorded and analyzed with laser confocal microscope.

4.14. Detection of Intracellular Generate Reactive (ROS)

Human lung cancer A549 cells (2×10^6 cells/mL) were incubated in six-well plates and allowed to coherent overnight, then treated with various compound: vehicle (DMF), cisplatin (5 µM), compound **20** (5 µM) and compound **26** (5 µM). After 24 h treatment, the cells were collected at 2000 rpm and washed twice with ice PBS. Subsequently, the tumor cells were incubated with DCFH-DA (Molecular Probe, Beyotime, Haimen, China) in dark at 37 °C for 30 min, following the instructions of kit. Finally, the results were analyzed with flow cytometry.

To investigate the specific reactive oxygen species, Mito-sox (KeyGEN BioTECH) was used as superoxide radical fluorescence probe, using excitation and emission wavelength of 510 nm and 595 nm, respectively. After 24 h treatment of

DMF, cisplatin (5 μM), **20** (5 μM) and **26** (5 μM), A549 cells were washed with cold PBS and stained with 5 μM Mito-sox for 15 min in dark at 37 °C. The results were recorded and analyzed with laser scanning confocal microscope.

4.15. Mitochondrial Membrane Potential ($\Delta\psi\text{m}$) depolarization assay

Human lung cancer A549 cells (2×10^6 cells/mL) were incubated in six-well plates and allowed to coherent overnight, then treated with various compound: vehicle (DMF), cisplatin (5 μM), compound **20** (5 μM) and compound **26** (5 μM). After 24 h treatment, the culture medium was removed, cells were washed with PBS two times and stained with JC-1 probe (KeyGen Biotech; KGA601-KGA604) for 20 min under 5% CO_2 at 37 °C following the instructions of test kit. Finally, cells were collected at 2500 rpm and washed twice with new ice PBS. The effects of various compounds on MMP of tumor cells were analyzed with confocal laser scanning microscope using 530 nm, 590 nm and 488 nm, 514 nm as emission fluorescence and excitation wavelength, respectively.

4.16. Cell morphology study

Human lung cancer A549 cells (1×10^6 cells/mL) were incubated in six-well plates and allowed to coherent overnight, then treated with various compound: vehicle (DMF), cisplatin (5 μM), compound **20** (5 μM) and compound **26** (5 μM). After incubation for 24 h, the cells were fixed with 4% paraformaldehyde for 10 min at room temperature and washed twice with cold PBS. After that, the cells were stained with 0.5 mL Hoechst 33258 or calcein-AM (500 μL , 2 μM) and PI (500 μL , 4 μM) double staining for 15 min in dark. After incubation, the cells were washed twice with cold PBS, the results were recorded with Nikon ECLIPSETE2000-S fluorescence microscope using 350 nm excitation and 460 nm emissions or confocal laser scanning microscope using 488 nm, 514 nm as excitation wavelength and 520 ± 20 nm, 640 ± 20 nm as emission wavelength.

4.17. Wound healing assay

Human lung cancer A549 cells (2×10^5 cells/mL) were incubated in six-well plates and allowed to coherent overnight. After about 90% confluence, wounds were

created with a p10 micropipette tip. Then the cells were washed twice with fresh PBS and added fresh media containing tested compounds, including control (DMF), CDDP (5 μ M), **20** (1 μ M) and **26** (1 μ M), respectively. All compounds were prepared in DMF and diluted to desired concentrations with media (without FBS supplementation). A549 cells were co-incubated for 24 h at 37 °C with tested compounds under serum-starved conditions. After 24 h treatment, the media was removed and washed twice with cold PBS and were fixed. The wound gaps were monitored and recorded photographically with by inverted microscope (Nikon) under 10 \times magnification.

4.18. Western blotting analysis

Freshly trypsinized A549 cells suspensions with a density of 3.0×10^4 cells/well were seeded in 6-well microtiter plates and incubated in atmosphere of 5% CO₂ and 95% air at 37.0 °C for overnight. Then, cisplatin, **20** and **26** dissolved in DMF and diluted to 5 μ M with medium were added respectively to the medium and incubated for 24 h at the same condition. Then the cells were collected, centrifuged and washed twice with ice PBS. The cells harvested above were lysed with a lysis buffer on ice for 30 min and centrifuged at 10000 g at 4°C for 5min. Protein amount of the cell lysates were measured with BCA protein assay reagents (Imgenex, USA) under the instructions of manufacture. Equal amount of total cellular protein extract was separated by electrophoresis on SDS–polyacrylamide gels and transferred to PVDF membranes. After blocking with 5% nonfat milk, the membrane was co-incubated with primary antibodies (anti-Bcl-2, anti-Bax, anti-Cyt c, anti-cleaved-caspase-9, anti-cleaved-caspase -3, anti-cleaved-PARP, anti-p53, anti- γ H2AX and anti- β -actin) at 4°C for overnight. Subsequently, the membrane was incubated with second antibodies conjugated with peroxidase for 2h, washed three times with TBST buffer for 15 min and visualized with chemiluminescence reagent (Thermo Fischer Scientifics Ltd.).

4.19. Antitumor assay in vivo

Six-week-old female BALB/c athymic nude mice with weight about 18.0 g were purchased from Shanghai Slac Laboratory Animal Co., Ltd. (China) and housed under

specific pathogen-free conditions following the guidance for the Care and Use of Laboratory Animals. A549 cells (3×10^6) in 100 μL of sterile PBS were injected subcutaneously in the flank of mice to generate A549 xenograft tumor models. After the tumor volume reached to 150-250 mm^3 , the mice ($n=3$) were sorted into four different groups with similar mean tumor size as follows: Normal saline, **20**, **26** and CDDP. All compounds dissolved in a mixture of 0.1% Tween-80 and normal saline were administrated via injecting intravenously through tail vein with a dose of 6 $\mu\text{mol/kg}$ on days of 0,2,4. Similarly, the mice in control group received equivalent volume of normal saline injection. Tumor volume were measured through a caliper and calculated according to the formula: Tumor volume (mm^3) = $A \times B^2 \times 0.5$, where A represented length and B was width. Body weight was measured and recorded 2-3 times every week. At the end of the experiment, all mice were sacrificed and the tumor were harvested for further study. Curves of tumor growth and body weights were plotted using the average data at the same group by origin 9.0.

Notes

The authors declare that they have no conflicts of interest.

Acknowledgements

The authors want to show thanks for the Natural Science Foundation of Guangxi Province (AB17292075,2016GXNSFGA380005) and Guangxi Funds for Distinguished Experts. Besides, we are grateful to the National Natural Science Foundation of China (Grant No. 21571033) and Priority Academic Program Development of Jiangsu Higher Education Institutions for the construction of fundamental facilities (Project 1107047002) for financial support of this study. Dr. Fang is thankful to the support of the State Key Laboratory for Chemistry and Molecular Engineering of Medicinal Resources (Guangxi Normal University) (CMEMR2017-B05), “Qing-Lan” project in Colleges and Universities of Jiangsu Province, the National Major Science and Technology Projects of China, and the Priority Academic Program Development of Jiangsu Higher Education Institutions.

Appendix A. Supplementary data

Figures of HPLC analysis of the stability and activation of **26** by reduction. DNA platination and gel electrophoretic assays. Microscale thermophoresis (MST) analysis of **20** and **26**. Cellular thermal shift assays (CETSA) of **26**. DNA damage induced by **26**. Detection of mitochondrial ROS. Table of antitumor activity of compound **26** on A549 xenograft models. HR-MS, ¹H-NMR, ¹³C-NMR, ¹⁹⁵Pt and TG spectra of intermediate or target compounds. HPLC purities results of target compounds (**11-14**, **19-28**).

Supplementary data related to this article can be found via the internet at .

Abbreviations used

MAPK, mitogen-activated protein kinase; RAS.GDP, GDP-bound state of RAS; RAS.GTP, GTP-bound state of RAS; ERK, extracellular signal-regulated kinase; CDDP, cisplatin; Oxa, oxaliplatin; A549/CDDP, cisplatin resistant human non-small cell lung cancer cells; SKOV3/CDDP, cisplatin resistant ovarian cancer cells; LO2, human normal liver cells; HUVEC, human umbilical vein endothelial cells; GAPs, GTPase-activating proteins; MEK1 and MEK2, mitogen-activated protein kinase kinases 1 and 2; RF, resistance factor; TBTU, O-(benzotriazol-1-yl)-N,N,N',N'-tramethyluronium tetrafluoroborate; TLC, Thin Layer Chromatography; DCM, dichloromethane; DMF, N,N-Dimethylformamide; TGA, 2-Mercaptoacetic acid; RP-HPLC, reverse-phase high performance liquid phase; MDR, multi-drug resistance; ICP-MS, inductively coupled plasma mass spectrometry; ROS, reactive oxygen species; PI, propidium iodide; MMP, mitochondrial membrane potential; AO/EB, acridine orange/ ethidium bromide; Cyt c, cytochrome C; Bcl-2, B-cell lymphoma-2 protein; Bax, Bcl-2 Associated X Protein; PARP, poly ADP-ribose polymerase; UV, ultraviolet; γ H2AX, phosphorylation of H2AX; DMEM, dulbecco's modified eagle medium; FACS, fluorescence-activated cell sorting; SDS-PAGE, sodium dodecyl sulfate polyacrylamide gel electrophoresis; IR, inhibition rate; TG, thermogravimetric.

References

- [1] A.E. Karnoub, R.A. Weinberg, Ras oncogenes: split personalities, *Nat. Rev. Mol. Cell Biol.* 9 (2008) 517–531.

- [2] K.L. Bryant, J.D. Mancias, A.C. Kimmelman, C.J. Der, KRAS: feeding pancreatic cancer proliferation, *Trends Biochem, Sci.* 39 (2014) 91–100.
- [3] Y. Pylayeva-Gupta, E. Grabocka, D. Bar-Sagi, RAS oncogenes: weaving a tumorigenic web, *Nat. Rev. Cancer.* 11 (2011) 761–774.
- [4] P. Crespo, J. Leon, Ras Proteins in the control of the cell cycle and cell differentiation, *Cell. Mol. Life Sci.* 57 (2000) 1613–1636.
- [5] M.V. Milburn, L. Tong, A.M. Devos, A.T. Brünger, Z. Yamaizumi, S. Nishimura, K. Sangjin, S.H. Kim, Molecular switch for signal transduction: structural differences between active and inactive forms of protooncogenic ras proteins, *Science* 247 (1990) 939–945.
- [6] I.R. Vetter, A. Wittinghofer, The guanine nucleotide-binding switch in three dimensions, *Science* 294 (2001) 1299–1304.
- [7] A.D. Luca, M.R. Maiello, A. D'Alessio, M. Pergameno, N. Normanno, The RAS/RAF/MEK/ERK and the PI3K/AKT signalling pathways: role in cancer pathogenesis and implications for therapeutic approaches, *Expert Opin. Ther. Targets* 16 (2012) S17–S27.
- [8] A. Young, D. Lou, F. McCormick, Oncogenic and wild-type Ras play divergent roles in the regulation of mitogen-activated protein kinase signaling, *Cancer Discov.* 3 (2013) 112–123.
- [9] A. Wittinghofer, K. Scheffzek, M.R. Ahmadian, The interaction of Ras with GTPase-activating proteins, *FEBS Lett.* 410 (1997) 63–67.
- [10] H.R. Bourne, D.A. Sanders, F. McCormick, The GTPase superfamily: a conserved switch for diverse cell function, *Nature* 348(1990) 125–132.
- [11] J.L. Bos, Ras oncogenes in human cancer: a review, *Cancer Res.* 49 (1989) 4682–4689.
- [12] I.A. Prior, P.D. Lewis, C. Mattos, A comprehensive survey of Ras mutations in cancer, *Cancer Res.* 72 (2012) 2457–2467.
- [13] S.M. Lim, K.D. Westover, S.B. Ficarro, R.A. Harrison, H.G. Choi, M.E. Pacold, M. Carrasco J. Hunter, N.D. Kim, T. Xie, T. Sim, P.A. Jänne, M. Meyerson, J.A.

Marto, J.R. Engen, N.S. Gray, Therapeutic targeting of oncogenic K-Ras by a covalent catalytic site inhibitor, *Angew. Chem. Int. Ed. Engl.* 126 (2014) 203–208.

[14] M.J. Smith, M. Ikura, Integrated RAS signaling defined by parallel NMR detection of effectors and regulators, *Nat. Chem. Biol.* 10 (2014) 223–230.

[15] S.K. Athuluri-divakar, R.V. Carpio¹, K. Dutta, S.J. Baker, S.C. Cosenza, I. Basue, Y.K. Gupta, M.V.R. Reddy, L. Ueno, J.R. Hart, P.K. Vogt, D. Mulholland, C. Guha, A.K. Aggarwal, E.P. Reddy, A small molecule RAS-mimetic disrupts RAS association with effector proteins to block signaling, *Cell* 165 (2016) 643–655.

[16] F. Shima, Y. Yoshikawa, M. Ye, M. Araki, S. Matsumoto, J. Liao, L. Hu, T. Sugimoto, Y. Ijiri, A. Takeda, Y. Nishiyama, C. Sato, S. Muraoka, A. Tamura, T. Osoda, K.I. Tsuda, T. Miyakawa, H. Fukunishi, J. Shimada, T. Kumasaka, M. Yamamoto, T. Kataoka, In silico discovery of small-molecule Ras inhibitors that display antitumor activity by blocking the Ras–effector interaction, *Proc. Natl. Acad. Sci. U.S.A.* 110 (2013) 8182–8187.

[17] A.D. Cox, S.W. Fesik, A.C. Kimmelman, J. Luo, C.J. Der, Drugging the undruggable RAS: mission possible? *Nat. Rev. Drug Discov.* 13 (2014) 828–851.

[18] J. Downward, Targeting RAS signaling pathways in cancer therapy, *Nat. Rev. Cancer* 3 (2003) 11–22.

[19] L. Santarpia, S.L. Lippman, A.K. El-Naggar, Targeting the mitogen-activated protein kinase RAS-RAF signaling pathway in cancer therapy, *Expert. Opin. Ther. Targets* 16 (2012) 103–119.

[20] M.V.R. Reddy, M. Mallireddigari, S. Cosenza, V. Pallela, N. Iqbal, K. Robell, A. Kang, E.P. Reddy, Design synthesis, and biological evaluation of (E)-styrylbenzyl sulfones as novel anticancer agents, *J. Med. Chem.* 51 (2008) 86–100.

[21] I. Park, M.V.R. Reddy, E.P. Reddy, J.E. Groopman, Evaluation of novel cell cycle inhibitors in mantle cell lymphoma, *Oncogene* 26 (2007) 5635–5642.

[22] K.D. Mjos, C. Orvig, Metallodrugs in medicinal inorganic chemistry, *Chem. Rev.* 114 (2014) 4540–4563.

[23] B. Rosenberg, L. Vancamp, J.E. Trosko, V.H. Mansour, Platinum compounds: a

- new class of potent anti-tumor agents, *Nature* 222 (1969), 385–386.
- [24] X. Y. Wang, X. H. Wang, Z.J. Guo, Functionalization of platinum complexes for biomedical applications, *Acc. Chem. Res.* 48 (2015) 2622–2631.
- [25] F. Liu, S. Gou, F. Chen, L. Fang, J. Zhao, Study on antitumor platinum(II) complexes of chiral diamines with dicyclic species as steric hindrance, *J. Med. Chem.* 58 (2015) 6368–6377.
- [26] M.A. Fuertes, C. Alonso, J.M. Perez, Biochemical modulation of cisplatin mechanisms of action: enhancement of antitumor activity and circumvention of drug resistance, *Chem. Rev.* 103 (2003) 645–662.
- [27] A.V. Klein, T.W. Hambley, Platinum drug distribution in cancer cells and tumors, *Chem. Rev.* 109 (2009) 4911–4920.
- [28] T. Johnstone, K. Suntharalingam, S.J. Lippard, The next generation of platinum drugs: targeted Pt(II) agents, nanoparticle delivery, and Pt(IV) prodrugs, *Chem. Rev.* 116 (2016) 3436–3486.
- [29] D. Wang, S.J. Lippard, Cellular processing of platinum anticancer drugs, *Nat. Rev. Drug Discov.* 4 (2005) 307–320.
- [30] D. Mukherjea, L.P. Rybak, K.E. Sheehan, T. Kaur, V. Ramkumar, S. Jajoo, S. Sheth, The design and screening of drugs to prevent acquired sensorineural hearing loss, *Expert. Opin. Drug Discov.* 6 (2011) 491–505.
- [31] X. Wang, X. Wang, S. Jin, N. Muhammad, Z. Guo, Stimuli-responsive therapeutic metallodrugs, *Chem. Rev.* 119 (2019) 1138–1192.
- [32] Z. Xu, W. Hu, Z. Wang, S. Gou, Platinum(IV) prodrugs multiply targeting genomic DNA, histone deacetylases and PARP-1, *Eur. J. Med. Chem.* 141 (2017) 211–220.
- [33] M.D. Hall, H.R. Mellor, R. Callaghan, T.W. Hambley, Basis for design and development of platinum(IV) anticancer complexes, *J. Med. Chem.* 50 (2007) 3403–3411.
- [34] M.D. Hall, T.W. Hambley, Platinum(IV) antitumour compounds: their bioinorganic chemistry, *Coord. Chem. Rev.* 232 (2002) 49–67.

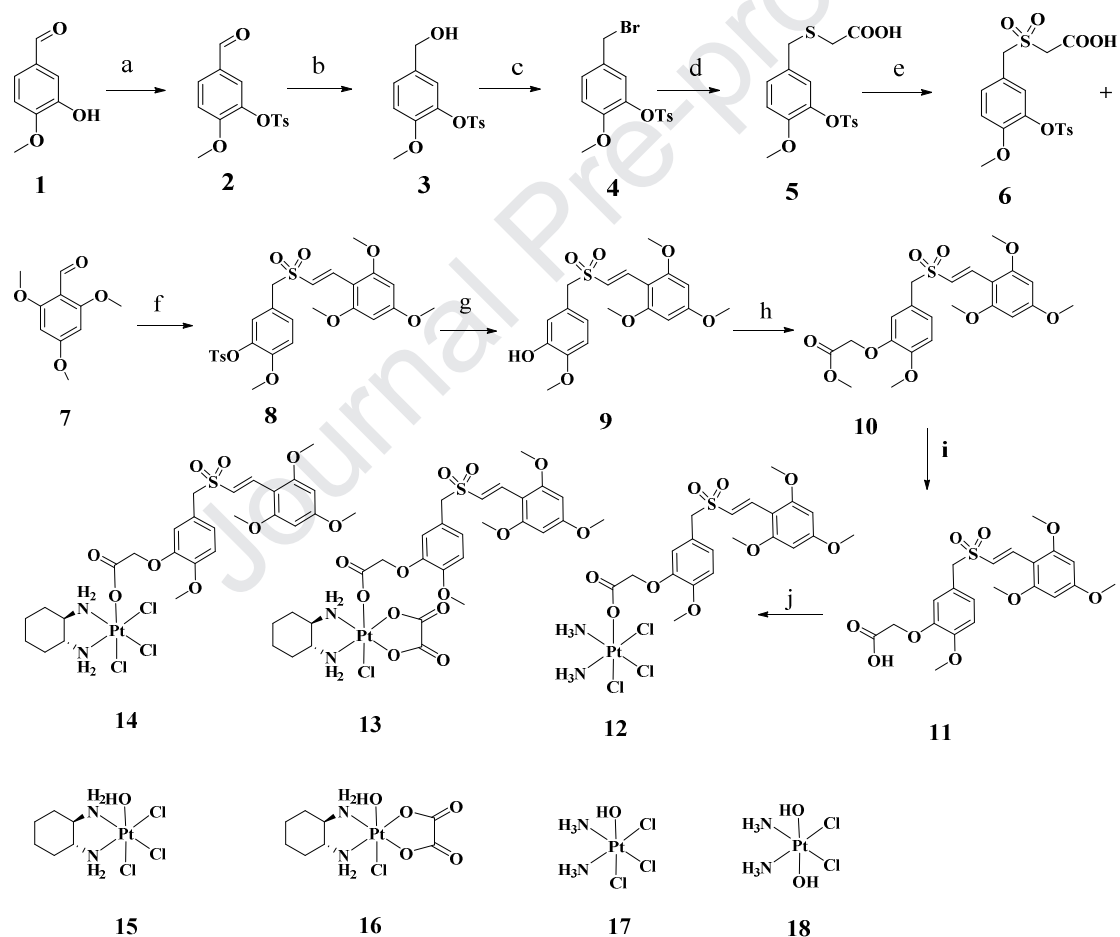
- [35] V. Venkatesh, P. J. Sadler, Platinum(IV) prodrugs, *Met. Ions Life Sci.* 18 (2018) 69–108.
- [36] U. Basu, B. Banik, R. Wen, R.K. Pathak, S. Dhar, The platin-X series: activation, targeting, and delivery, *Dalton Trans.* 45 (2016) 12992–13004.
- [37] X. Qin, L. Fang, F. Chen, S. Gou, Conjugation of Pt(IV) complexes with chlorambucil to overcome cisplatin resistance via a "joint action" mode toward DNA, *Eur. J. Med. Chem.* 137 (2017) 167–175.
- [38] X. Huang, R. Huang, S. Gou, Z. Wang, H. Wang, Anticancer platinum(IV) prodrugs containing monoaminophosphonate ester as a targeting group inhibit matrix metalloproteinases and reverse multidrug resistance, *Bioconjugate Chem.* 28 (2017) 1305–1323.
- [39] X. Huang, R. Huang, S. Gou, Z. Wang, Z. Liao, H. Wang, Pt(IV) complexes conjugated with phenstatin analogue as inhibitors of microtubule polymerization and reverser of multidrug resistance, *Bioorg. Med. Chem.* 137 (2017) 167–175.
- [40] M.V.R. Reddy, P. Venkatapuram, M.R. Mallireddigari, V.R. Pallela, S.C. Cosenza, K.A. Robell, B. Akula, B.S. Hoffman, E.P. Reddy, Discovery of a clinical stage multi-kinase inhibitor sodium (E)-2-{2-Methoxy-5-[(2',4',6'-trimethoxystyryl sulfonyl) methyl]phenylaminoacetate (ON01910.Na):synthesis, structure–activity relationship, and biological activity, *J. Med. Chem.* 54 (2011) 6254–6276.
- [41] M.V.R. Reddy, M.R. Mallireddigari, S.C. Cosenza, V.R. Pallela, N.M. Iqbal, K.A. Robell, A.D. Kang, E.P. Reddy, Synthesis, and biological evaluation of (E)-Styrylbenzylsulfones as novel anticancer agents, *J. Med. Chem.* 51 (2008) 86–100.
- [42] R.J. Schilder, F.P. Lacreta, R.P. Perez, S.W. Johnson, J.M. Brennan, A. Rogatko, S. Nash, C. Mcaleer, T.C. Hamilton, D. Roby, R.C. Young, R.F. Ozols, P. J. O'Dwyer, Phase I and pharmacokinetic study of ormaplatin (Tetraplatin, NSC 363812) administered on a day 1 and day 8 schedule, *Cancer Res.* 54 (1994) 709–717.
- [43] A. Bhargava, U.N. Vaishampayan, Satraplatin: leading the new deneration of oral platinum agents, *Expert Opin. Inv. Drug.* 18 (2009) 1787–1797.

- [44] M.A. Fuertes, C. Alonso, J.M. Perez, Biochemical modulation of cisplatin mechanisms of action: enhancement of antitumor activity and circumvention of drug resistance, *Chem. Rev.* 103 (2003) 645–662.
- [45] F. Gümüş, G. Eren, L. Açık, A. Çelebi, F. Öztürk, S. Yılmaz, R.I. Sagkan, S. Gür, A. Özkul, A. Elmalı, Y. Elerman, Synthesis, Cytotoxicity, and DNA Interactions of New Cisplatin Analogues Containing Substituted Benzimidazole Ligands, *J. Med. Chem.* 52 (2009) 1345–1357.
- [46] M.V. Keck, S.J. Lippard, Unwinding of supercoiled DNA by platinum-ethidium and related complexes, *J. Am. Chem. Soc.* 114 (1992) 3386–3390.
- [47] R. Li, X. Luo, Y. Zhu, L. Zhao, L. Li, Q. Peng, M. Ma, Y. Gao, ATM signals to AMPK to promote autophagy and positively regulate DNA damage in response to cadmium-induced ROS in mouse spermatocytes, *Environ. Pollut.* 231 (2017) 1560–1568.
- [48] A. Kyziol, A. Cierniak, J. Gubernator, A. Markowski, M. Jezowska-Bojczuk, U.K. Komarnicka, Copper(I) complexes with phosphine derived from sparfloxacin. Part III: multifaceted cell death and preliminary study of liposomal formulation of selected copper(I) complexes, *Dalton Trans.* 47 (2018) 1981–1992.
- [49] Y. Li, Q. Wu, G. Yu, L. Li, X. Zhao, X. Huang, W. Mei, Polypyridyl Ruthenium(II) complex-induced mitochondrial membrane potential dissipation activates DNA damage-mediated apoptosis to inhibit liver cancer, *Eur. J. Med. Chem.* 164 (2019) 282–291.
- [50]. K.T. Papazisis, D. Zambouli, O.T. Kimoundri, E. S. Papadakis, V. Vala, G. D.Geromichalos, S. Voyatzi, D. Markala, E., Destouni, L. Boutis, Protein tyrosine kinase inhibitor, genistein, enhances apoptosis and cell cycle arrest in K562 cells treated with γ -irradiation, *Cancer Lett.* 160 (2000) 107–113.
- [51]. Y. Li, L.P. Zhang, F. Dai, W.J. Yan, H.B. Wang, Z.S. Tu, B. Zhou, Hexamethoxylated monocarbonyl analogues of curcumin cause G2/M cell cycle arrest in NCI-H460 cells via michael acceptor-dependent redox intervention, *J. Agric. Food Chem.* 63 (2015) 7731–7742.

- [52] S.J. Dougan, A. Habtemariam, S.E. Mchale, S. Parsons, P.J. Sadler, Catalytic organometallic anticancer complexes, *Proc. Natl. Acad. Sci. U.S.A.* 105 (2008) 11628–11633.
- [53] Y. Fu, M.J. Romero, A. Habtemariam, M.E. Snowden, L. Song, G.J. Clarkson, B. Qamar, A.M. Pizarro, P.R. Unwin, P.J. Sadler, The contrasting chemical reactivity of potent isoelectronic iminopyridine and azopyridine osmium(II) arene anticancer complexes, *Chem. Sci.* 3 (2012) 2485–2494.
- [54] B. Kalyanaraman, V. Darley-Usmar, K.J.A. Davies, P.A. Dennerly, H.J. Forman, M.B. Grisham, G.E. Mann, K. Moore, L.J. Roberts II, H. Ischiropoulos, Measuring reactive oxygen and nitrogen species with fluorescent probes: challenges and limitations, *Free Radical Bio. Med.* 52 (2012) 1–6.
- [55] Y. Tsutsumishita, T. Onda, K. Okada, M. Takeda, H. Endou, S. Futaki, M. Niwa, Involvement of H₂O₂ production in cisplatin induced nephrotoxicity, *Biochem. Biophys. Res. Commun.* 242 (1998) 310–312.
- [56] H. Masuda, T. Tanaka, U. Takahama, Cisplatin generates superoxide anion by interaction with DNA in a cell-free system, *Biochem. Biophys. Res. Commun.* 203 (1994) 1175–1180.
- [57] F. Dai, Q. Li, Y. Wang, C. Ge, C. Feng, S. Xie, H. He, X. Xu, C. Wang, Design, synthesis, and biological evaluation of mitochondria-targeted flavone-naphthalimide-polyamine conjugates with antimetastatic activity, *J. Med. Chem.* 60 (2017) 2071–2083.
- [58] R. Quintana-Cabrera, S. Fernandez-Fernandez, V. Bobo-Jimenez, J. Escobar, J. Sastre, A. Almeida, J.P. Bolanos, gamma-Glutamylcysteine detoxifies reactive oxygen species by acting as glutathione peroxidase-1 cofactor, *Nat. Commun.* 3 (2012) 718.
- [59] L. Macchioni, M. Petricciuolo, M. Davidescu, K. Fettucciari, P. Scarpelli, R. Vitale, L. Gatticchi, P.L. Orvietani, A. Marchegiani, P. Marconi, G. Bassotti, A. Corcelli, L. Corazzi, Palmitate lipotoxicity in enteric glial cells: Lipid remodeling and mitochondrial ROS are responsible for cyt c release outside mitochondria, *BBA-Mol. Cell Biol. L.* 1863 (2018) 895–908.

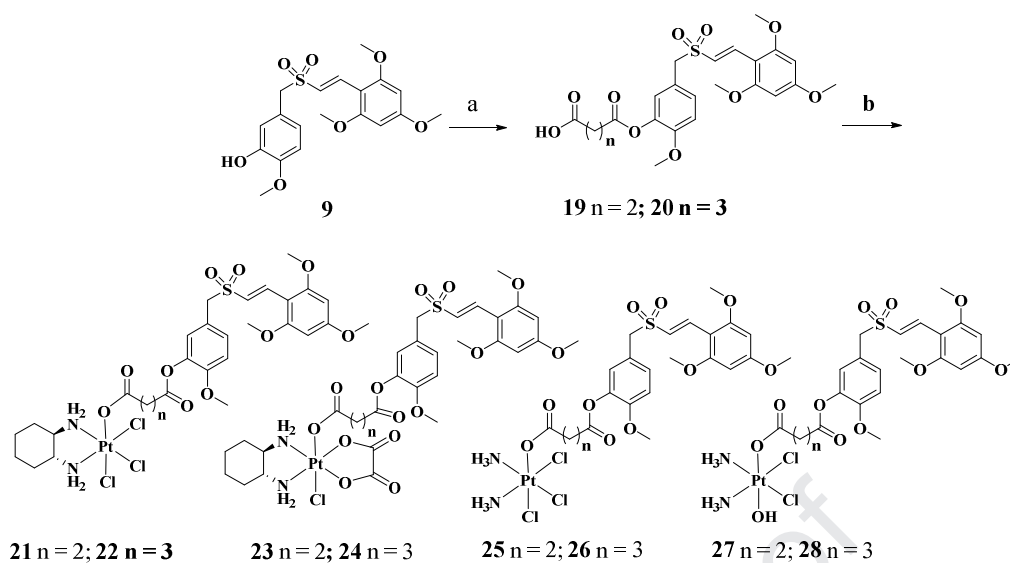
- [60] B.C. Bohrens, T.C. Hamilton, H. Masuda, K.R. Grotzinger, J. Whang-Peng, K. G. Louie, T. Knutsen, W.M. McKoy, R.C. Young, R.F. Ozols, Characterization of a cis-diamminedichloroplatinum(II)-resistant human ovarian cancer cell line and its use in evaluation of platinum analogues, *Cancer Res.* 47 (1987) 414–418.
- [61] H.M. Coley, W.B. Amos, P.R. Twentyman, P. Workman, Examination by laser scanning confocal fluorescence imaging microscopy of the subcellular localization of anthracyclines in parent and multidrug resistant cell lines, *Br. J. Cancer* 67 (1993) 1316–1323.
- [62] M.J. McCarthy, C.V. Pagba, P. Prakash, A.K. Naji, D.V.D. Hoeven, H. Liang, A. K. Gupta, Y. Zhou, K.J. Cho, J.F. Hancock, A.A. Gorfe, Discovery of high-affinity noncovalent allosteric KRAS Inhibitors that disrupt effector binding, *ACS Omega* 4 (2019) 2921–2930.

Scheme 1.



Reagents and conditions: a) TsCl, Et₃N, DCM; b) NaHB₄, DCM, MeOH; c) PBr₃, DCM; d) TGA, NaOH, MeOH; e) H₂O₂, AcOH; f) Piperidine, Benzoic acid, Toluene; g) NaOH, MeOH; h): Ethyl bromoacetate, K₂CO₃, DMF, KI; i): LiOH·H₂O, MeOH, H₂O; j) **15/16/17/18**, TBTU, Et₃N, DMF.

Scheme 2



Reagents and conditions: a) Succinic anhydride or glutaric anhydride, K_2CO_3 , DMF; b)

15/16/17/18, TBTU, Et_3N , DMF.

Journal Pre-proof

Figure captions:

Figure 1. FDA approved anticancer metallodrugs, platinum(IV) complexes in clinical trials and structures of Rigosertib and ON 013100.

Figure 2. Quantitative results cell uptake of **26** in A549 cells treated with **26** for 12 h at the concentration of 5 μM and 10 μM . Platinum content was measured by ICP-MS after digestion with 65% HNO_3 . Data represent the mean \pm SD of at least three replicates.

Figure 3. Propidium iodide/annexin V assay for the detection of apoptotic A549 cancer cells after treatment with DMF, CDDP (5 μM), **20** (2 μM , 5 μM), **26** (2 μM , 5 μM) for 24 h, respectively. The results showed the percentage of viable, apoptotic and dead cells.

Figure 4. Effect of compound **26** on CRAF phosphorylation, RAS-RAF interaction and MEK/ERK activation. (A) A549 cells were treated with **20** (5 μM) and **26** (5 μM) for 24 h and cell lysates were subjected to immunoprecipitation with anti-RAS antibodies and the associated CRAF was analyzed with western blot. (B) Signals were collected from western blot analysis of change in RAS and p-CRAF induced by **20** and **26**. Data were presented as the mean \pm s.d. of three independent experiments. (C) A549 cells were treated with CDDP (5 μM), **20** (2 μM), **20** (5 μM), **26** (2 μM) and **26** (5 μM) for 24 h and the level of MEK, p-MEK, ERK, p-ERK and GAPDH (loading control) were determined with western blot analysis. (D) Statistics of MEK, p-MEK, ERK and p-ERK. Signals were normalized with GAPDH. Data were presented as the mean \pm s.d. of three independent experiments.

Figure 5. FACS analysis of A549 cells treated with DMF, CDDP (5 μM), **20** (2 μM , 5 μM), **26** (2 μM , 5 μM) for 24 h. The results showed that cells treated with **20** and **26** were blocked in G2/M phase, whereas S phase of CDDP.

Figure 6. DNA damage in A549 cells induced by **26** and **20**. A549 cells were treated with CDDP (5 μM), **20** (5 μM) and **26** (5 μM) for 24 h and examined by comet assays. The longer tail of cells reflected the more severe damage of DNA in A549 cells. The tails of DNA were marked with white arrows.

Figure 7. After 24 h treatment with vehicle (DMF), CDDP (5 μ M), **20** (5 μ M) and **26** (5 μ M), A549 cells were incubated with fluorescence probe DCFH-DA. Results were recorded and analyzed with flow cytometry (BD Biosciences).

Figure 8. **26** induced loss of mitochondrial membrane potential in A549 cells. After 24 h treatment with vehicle A (DMF), B (CDDP, 5 μ M), C (**20**, 5 μ M) and D (**26**, 5 μ M), A549 cells were incubated with JC-1 fluorescent probe. The increase of green fluorescent in A549 cells were shown, indicating occurrence of $\Delta\psi$ m depolarization.

Figure 9. Morphological changes of A549 cells induced by **26**. A549 cells were treated with various compounds of vehicle (DMF), CDDP (5 μ M), **20** (5 μ M) and **26** (5 μ M), respectively. After 24 h co-incubation, cells were fixed and stained with (A) hoechst 33258, (B) Calcein-AM (green, living cells) and (C) PI (red, dead cells). Results were analyzed and recorded with confocal laser scanning microscope.

Figure 10. Complex **26** prevented A549 cells migration. After overnight attachment, a wound was created by scratching with a pipette tip and the cells were co-incubated with control (DMF), CDDP (5 μ M), **20** (50 nM) and **26** (50 nM) for 24 h. These figures are representative of one experiment of three with similar results.

Figure 11. Effect of **26** on the activation of mitochondrial apoptotic pathway. (A) The Expression of Cyt c, Bcl-2, Bax, cleaved-caspase-9, cleaved-caspase-3 and cleaved-PARP were analyzed by western blot after A549 cells were treated with DMF, CDDP (5 μ M), **20** (5 μ M) and **26** (5 μ M) for 24 h. (B) Quantitative results of Cyt c, Bcl-2, Bax, cleaved-caspase-9, cleaved-caspase-3 and cleaved-PARP protein levels, which were adjusted to the β -actin protein level. Values represent the mean \pm SE of three independent experiments.

Figure 12. Antitumor activity of compound **26** on A549 xenograft models. Nude mice were

implanted with A549 cells in the flank. When the tumor volume reached to 150-250 mm³, the mice were sorted into four groups (n=3) and dosed via injecting intravenously of **26** (6 μmol/kg), **20** (6 μmol/kg), CDDP (6 μmol/kg), vehicle (equivalent volume of normal saline injection) on days 0, 2 and 4. The mice were sacrificed and made mathematical statistics. (A) Tumor pictures obtained after sacrifice of the mice treated with **26**, **20**, CDDP and vehicle. (B) The RTV (relative tumor volume) (± SEM) is graphed with error bars representing the standard deviation. (C) The average body weights (± SEM) were plotted after sacrifice of the mice treated with **26**, **20**, CDDP and vehicle.

Figure 13. The proposed multifunctional anti-tumor mechanism of **26**.

Tables:

Table 1. Anti-proliferative activity in vitro of novel Pt(IV) prodrugs.

Compds.	IC ₅₀ (μM)			
	A549	OVCaR-3	SGC-7901	HCT-116
9	0.029 ± 0.002	0.031 ± 0.004	0.026 ± 0.003	0.029 ± 0.003
11	22.55 ± 1.23	15.35 ± 1.12	16.25 ± 0.80	13.24 ± 0.91
12	5.65 ± 0.63	4.80 ± 0.45	3.82 ± 0.35	4.52 ± 0.25
13	12.88 ± 1.15	10.25 ± 1.10	10.11 ± 1.05	6.5 ± 0.85
14	5.97 ± 0.27	6.50 ± 0.30	6.01 ± 0.21	5.51 ± 0.71
19	0.020 ± 0.012	0.016 ± 0.003	0.022 ± 0.002	0.017 ± 0.002
20	0.012 ± 0.003	0.019 ± 0.003	0.029 ± 0.003	0.022 ± 0.002
21	0.028 ± 0.003	0.014 ± 0.003	0.015 ± 0.001	0.019 ± 0.002
22	0.018 ± 0.003	0.030 ± 0.002	0.022 ± 0.002	0.031 ± 0.003
23	0.022 ± 0.004	0.023 ± 0.002	0.026 ± 0.003	0.020 ± 0.002
24	0.018 ± 0.004	0.012 ± 0.003	0.031 ± 0.002	0.020 ± 0.002
25	0.011 ± 0.001	0.012 ± 0.001	0.011 ± 0.001	0.022 ± 0.002
26	0.008 ± 0.001	0.009 ± 0.002	0.010 ± 0.001	0.012 ± 0.003
27	0.018 ± 0.003	0.015 ± 0.002	0.016 ± 0.002	0.020 ± 0.001
28	0.027 ± 0.002	0.034 ± 0.003	0.012 ± 0.011	0.039 ± 0.003
CDDP/20 ^a	0.020 ± 0.002	0.041 ± 0.011	0.032 ± 0.021	0.046 ± 0.002
CDDP ^b	8.22 ± 0.91	7.21 ± 0.83	5.45 ± 1.26	9.05 ± 0.55
Oxa. ^c	11.95 ± 1.43	8.29 ± 0.76	12.06 ± 1.66	16.09 ± 2.44

CDDP/20^a, cisplatin :20 = 1:1; CDDP^b, cisplatin; Oxa.^c, oxaliplatin.

Table 2. Anti-proliferative activity in vitro of novel Pt(IV) prodrugs.

Comp.	^a IC ₅₀ (μM)							
	A549	A549 /CDDP	SKOV3	SKOV-3 /CDDP	HUEVC	LO2	^d RF1	^e RF2
20	0.012 ± 0.003	0.016 ± 0.008	0.035 ± 0.006	0.041 ± 0.009	182.80 ± 9.2	126.639 ± 7.5	1.3	1.2
26	0.008 ± 0.001	0.009 ± 0.003	0.055 ± 0.012	0.089 ± 0.005	9.38 ± 0.82	7.86 ± 1.85	1.1	1.6
^b CDDP/20	0.020 ± 0.005	0.035 ± 0.003	0.075 ± 0.004	0.14 ± 0.022	0.45 ± 0.07	1.45 ± 0.36	1.8	1.9
^c CDDP	8.22 ± 0.91	34.55 ± 1.09	7.45 ± 1.36	40.55 ± 2.32	9.45 ± 1.54	10.28 ± 2.65	4.2	5.4

^aIC₅₀, Values are means ± SD obtained from three independent experiments. ^bCDDP/20, CDDP : 20 = 1:1, n/n; cisplatin :20 = 1:1; ^cCDDP, cisplatin; ^dRF1, Resistance Factor = IC₅₀ (A549/CDDP)/IC₅₀ (A549); ^eRF2, Resistance Factor = IC₅₀ (SKOV-3/CDDP)/IC₅₀ (SKOV-3).

Figures:

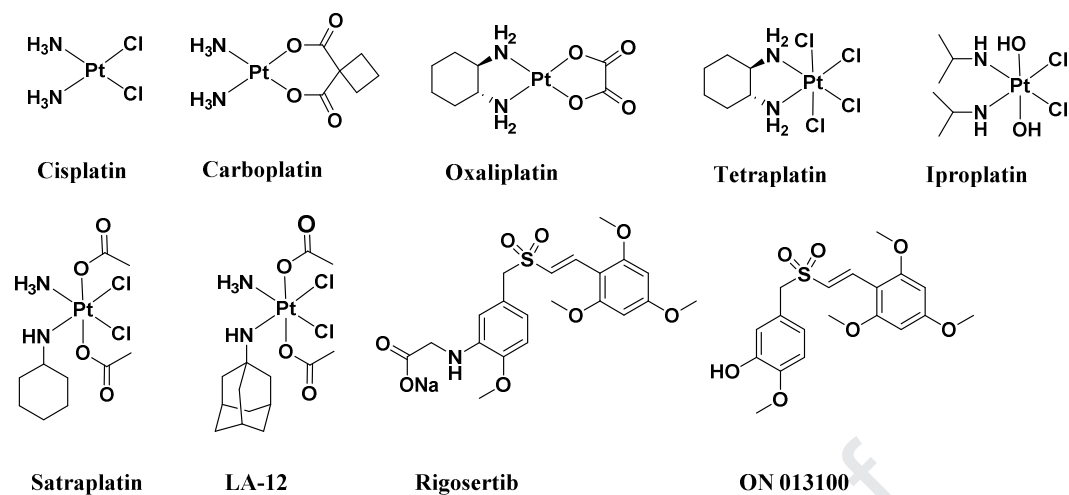


Figure 1. FDA approved anticancer metallodrugs, platinum(IV) complexes in clinical trials and structures of Rigosertib and ON 013100.

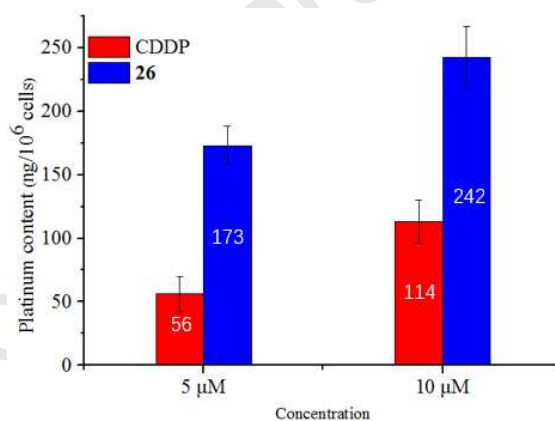


Figure 2. Quantitative results cell uptake of **26** in A549 cells treated with **26** for 12 h at the concentration of 5 μM and 10 μM. Platinum content was measured by ICP-MS after digestion with 65% HNO₃. Data represent the mean ± SD of at least three replicates.

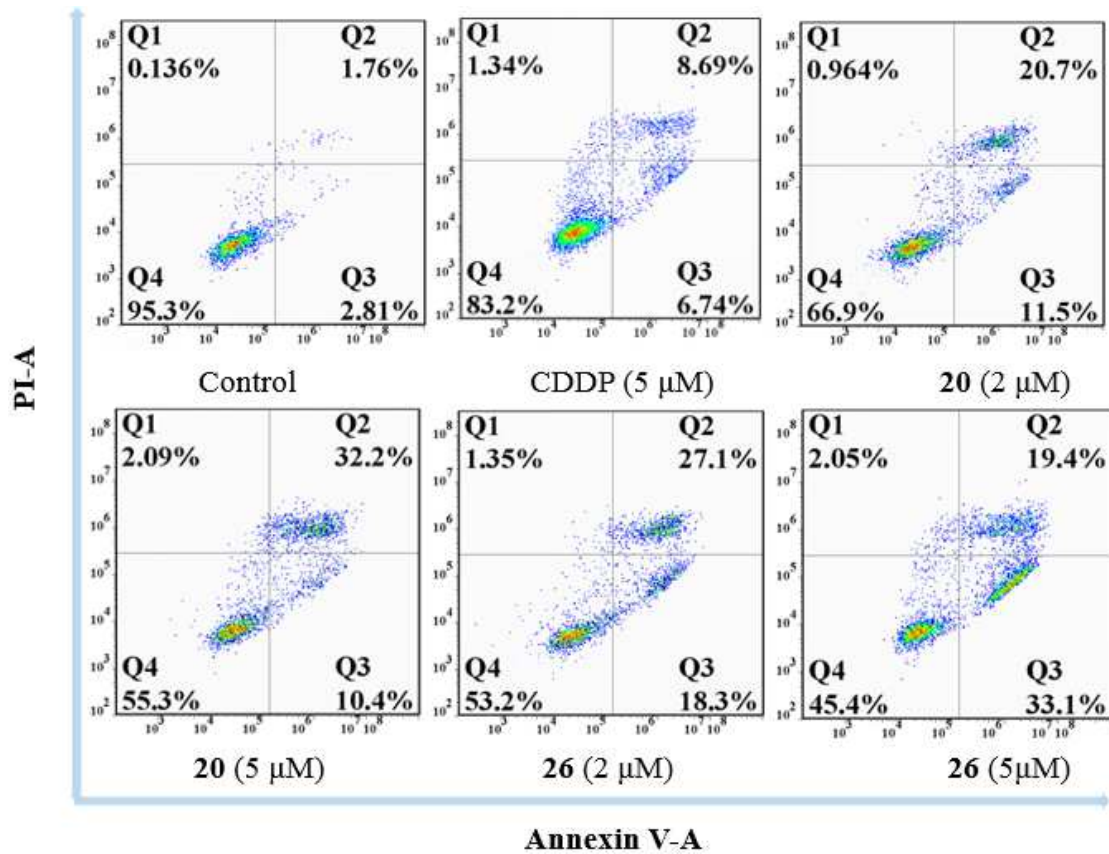


Figure 3. Propidium iodide/annexin V assay for the detection of apoptotic A549 cancer cells after treatment with DMF, CDDP (5 μ M), **20** (2 μ M, 5 μ M), **26** (2 μ M, 5 μ M) for 24 h, respectively. The results showed the percentage of viable, apoptotic and dead cells.

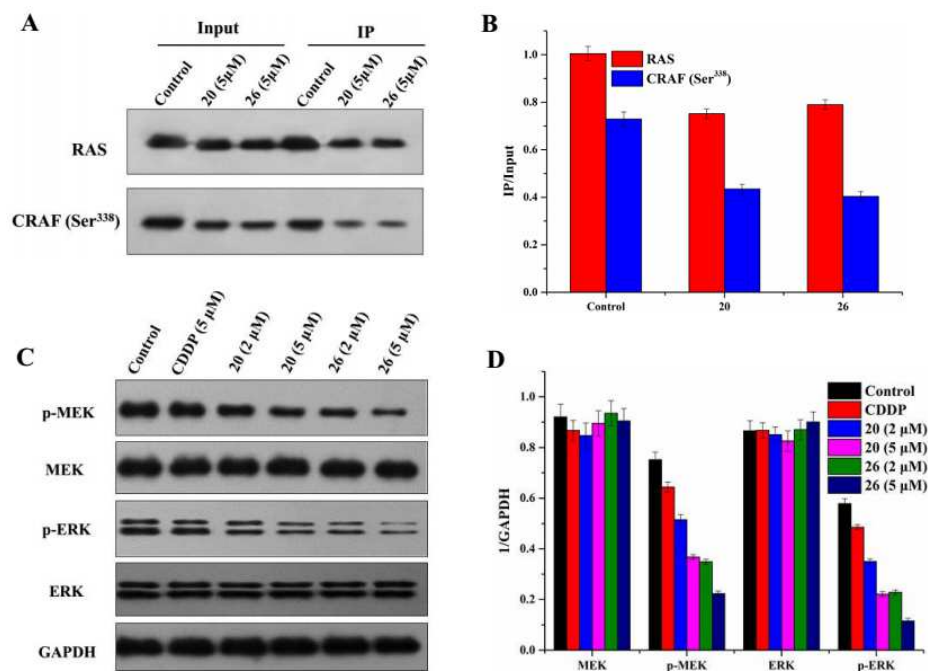


Figure 4. Effect of compound **26** on CRAF phosphorylation, RAS-RAF interaction and MEK/ERK activation. (A) A549 cells were treated with **20** (5 μ M) and **26** (5 μ M) for 24 h and cell lysates were subjected to immunoprecipitation with anti-RAS antibodies and the associated CRAF was analyzed with western blot. (B) Signals were collected from western blot analysis of change in RAS and p-CRAF induced by **20** and **26**. Data were presented as the mean \pm s.d. of three independent experiments. (C) A549 cells were treated with CDDP (5 μ M), **20** (2 μ M), **20** (5 μ M), **26** (2 μ M) and **26** (5 μ M) for 24 h and the level of MEK, p-MEK, ERK, p-ERK and GAPDH (loading control) were determined with western blot analysis. (D) Statistics of MEK, p-MEK, ERK and p-ERK. Signals were normalized with GAPDH. Data were presented as the mean \pm s.d. of three independent experiments.

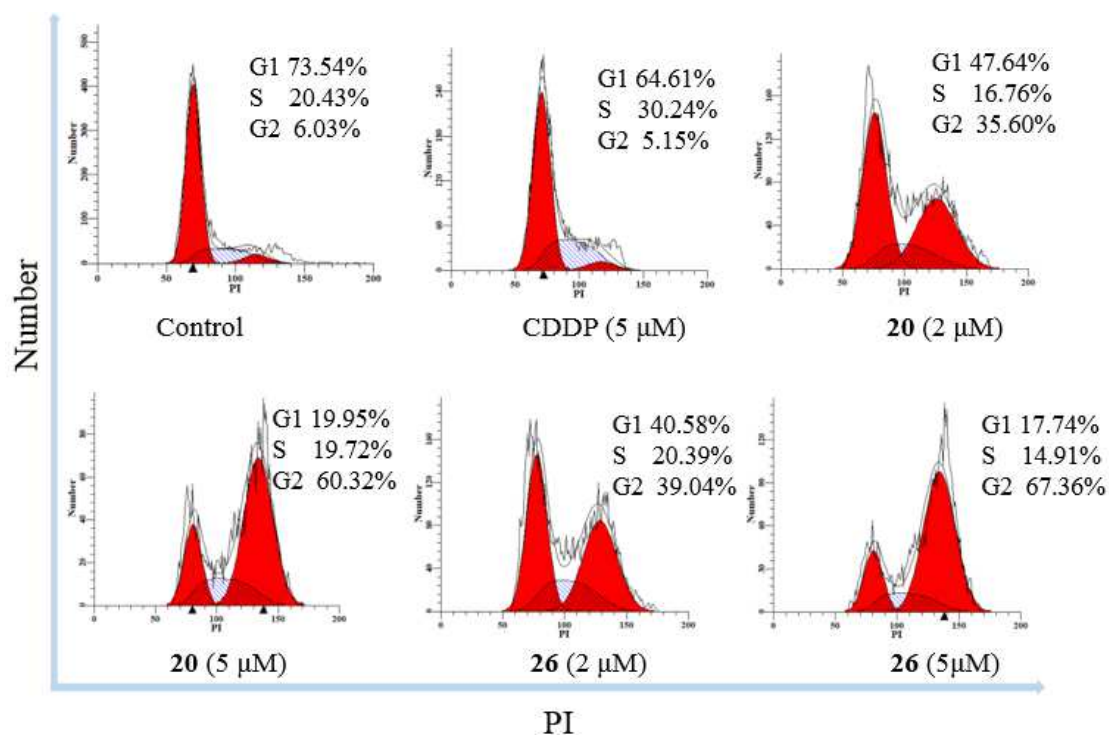


Figure 5. FACS analysis of A549 cells treated with DMF, CDDP (5 μ M), **20** (2 μ M, 5 μ M), **26** (2 μ M, 5 μ M) for 24 h. The results showed that cells treated with **20** and **26** were blocked in G2/M phase, whereas S phase of CDDP.

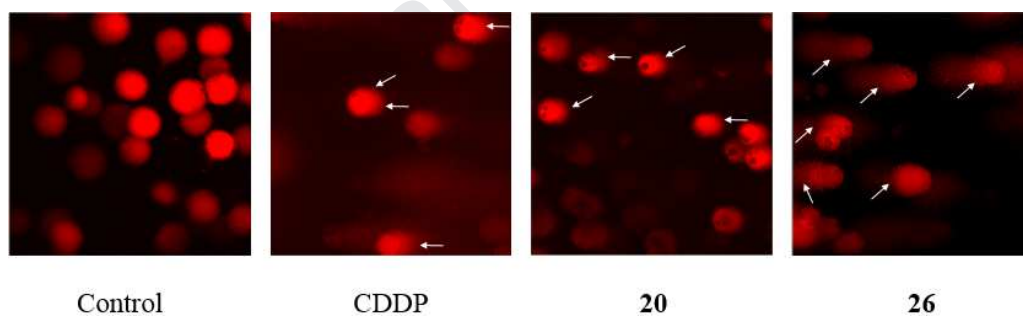


Figure 6. DNA damage in A549 cells induced by **26** and **20**. A549 cells were treated with CDDP (5 μ M) **20** (5 μ M) and **26** (5 μ M) for 24 h and examined by comet assays. The longer tail of cells reflected the more severe damage of DNA in A549 cells. The tails of DNA were marked with white arrows.

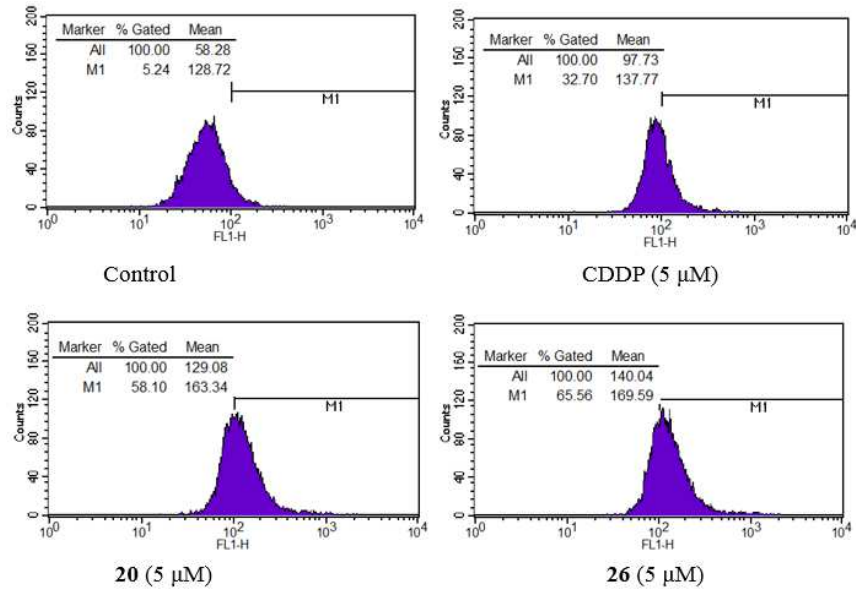
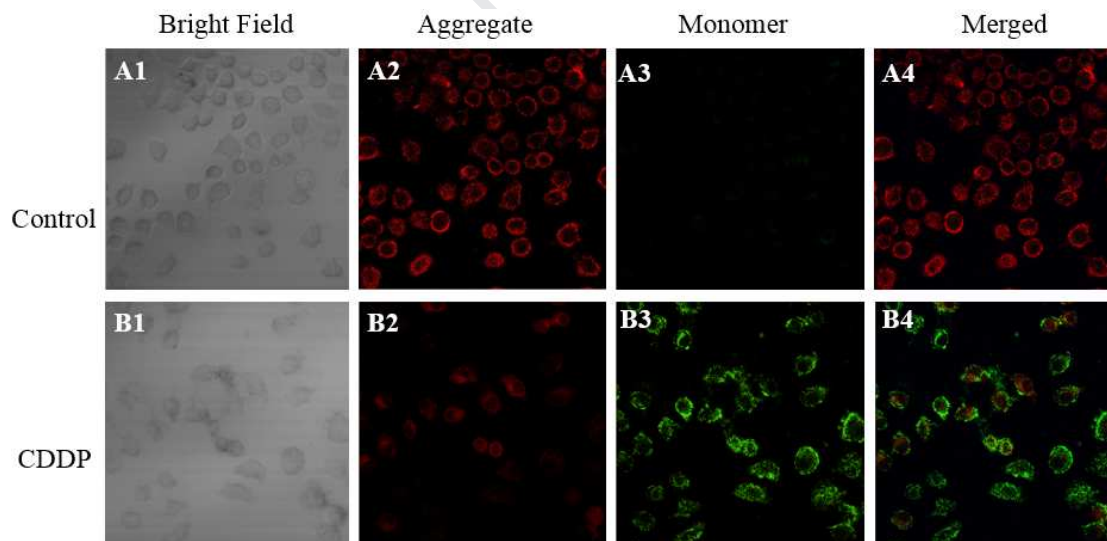


Figure 7. After 24 h treatment with vehicle (DMF), CDDP (5 μ M), **20** (5 μ M) and **26** (5 μ M), A549 cells were incubated with fluorescence probe DCFH-DA. Results were recorded and analyzed with flow cytometry (BD Biosciences).



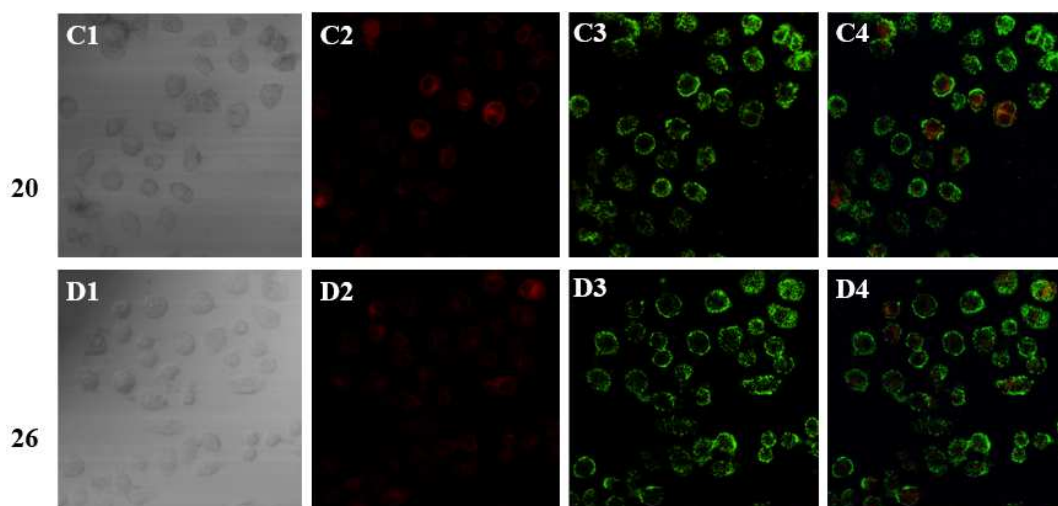


Figure 8. **26** induced loss of mitochondrial membrane potential in A549 cells. After 24 h treatment with vehicle A (DMF), B (CDDP, 5 μ M), C (**20**, 5 μ M) and D (**26**, 5 μ M), A549 cells were incubated with JC-1 fluorescent probe. The increase of green fluorescent in A549 cells were shown, indicating occurrence of $\Delta\psi_m$ depolarization.

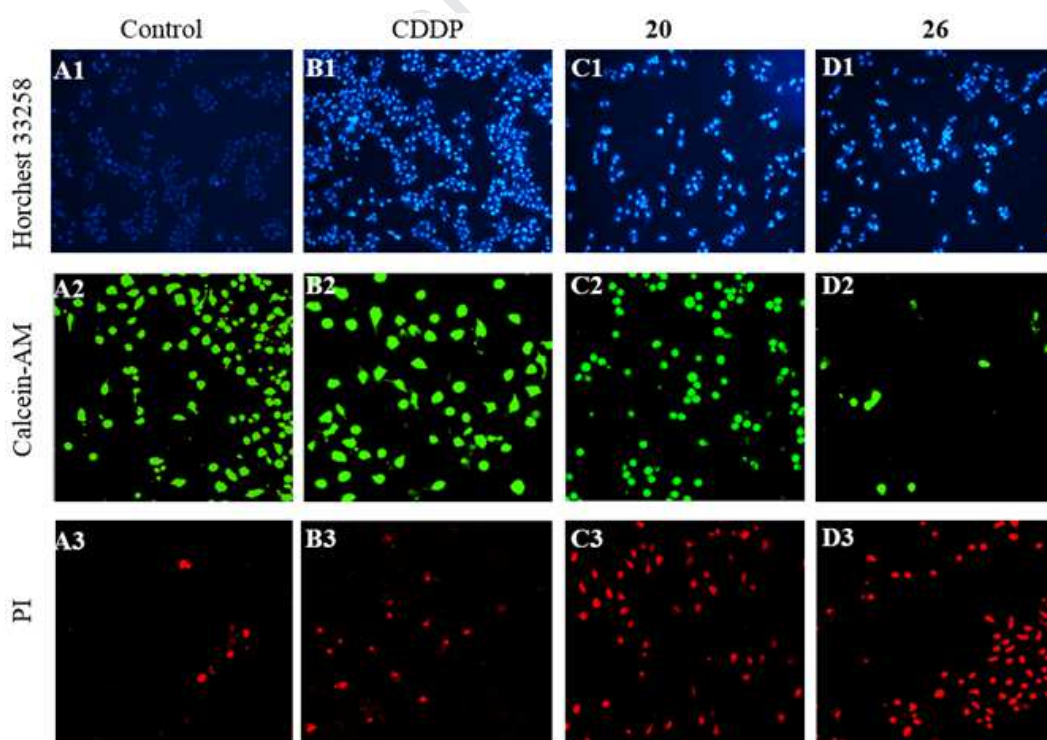


Figure 9. Morphological changes of A549 cells induced by **26**. A549 cells were treated with various compounds of vehicle (DMF), CDDP (5 μ M), **20** (5 μ M) and **26** (5 μ M), respectively. After 24 h co-incubation, cells were fixed and stained with (A1-D1) hoechst 33258, (A2-D2)

Calcein-AM (green, living cells) and (A3-D3) PI (red, dead cells). Results were analyzed and recorded with confocal laser scanning microscope.

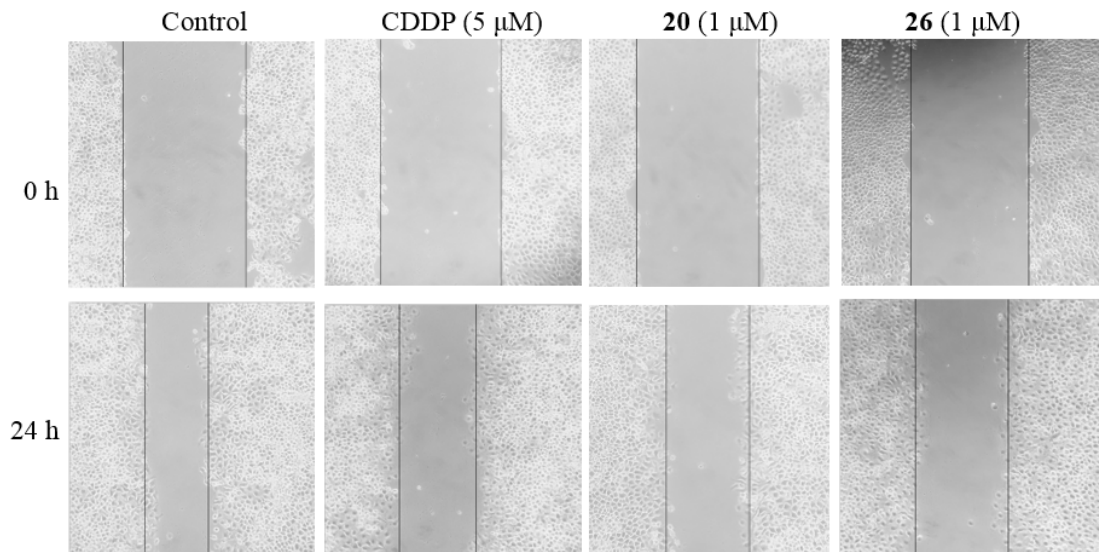


Figure 10. Complex **26** prevented A549 cells migration. After overnight attachment, a wound was created by scratching with a pipette tip and the cells were co-incubated with control (DMF), CDDP (5 μM), **20** (1 μM) and **26** (1 μM) for 24 h. These figures are representative of one experiment of three with similar results.

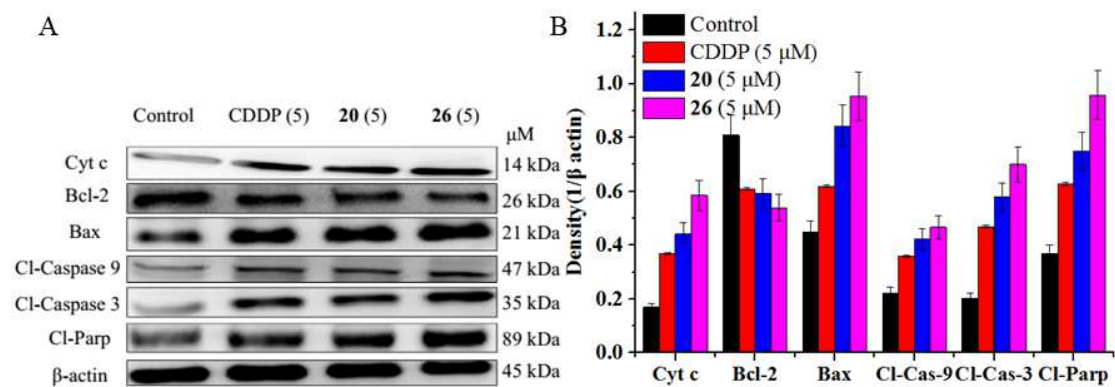


Figure 11. Effect of **26** on the activation of mitochondrial apoptotic pathway. (A) The Expression of Cyt c, Bcl-2, Bax, cleaved-caspase-9, cleaved-caspase-3 and cleaved-PARP were analyzed by

western blot after A549 cells were treated with DMF, CDDP (5 μ M), **20** (5 μ M) and **26** (5 μ M) for 24 h. (B) Quantitative results of Cyt c, Bcl-2, Bax, cleaved-caspase-9, cleaved-caspase-3 and cleaved-PARP protein levels, which were adjusted to the β -actin protein level. Values represent the mean \pm SE of three independent experiments.

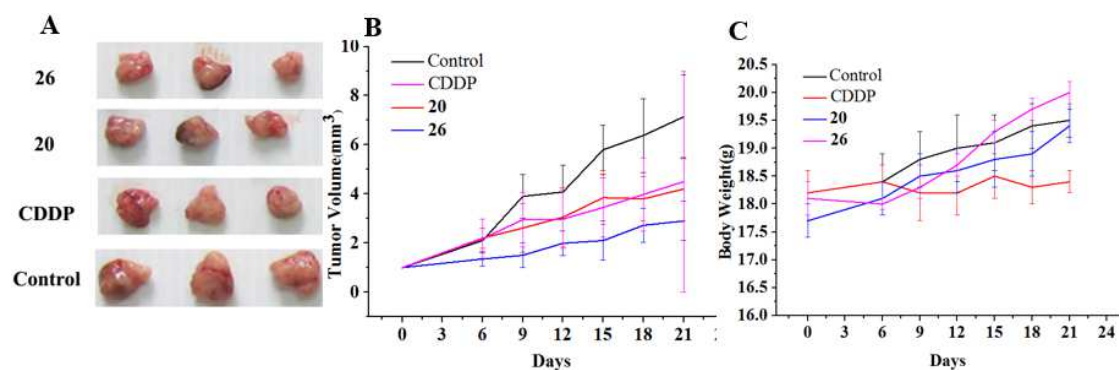


Figure 12. Antitumor activity of compound **26** on A549 xenograft models. Nude mice were implanted with A549 cells in the flank. When the tumor volume reached to 150-250 mm³, the mice were sorted into four groups (n=3) and dosed via injecting intravenously of **26** (6 μ mol/kg), **20** (6 μ mol/kg), CDDP (6 μ mol/kg), vehicle (equivalent volume of normal saline injection) on days 0, 2 and 4. The mice were sacrificed and made mathematical statistics. (A) Tumor pictures obtained after sacrifice of the mice treated with **26**, **20**, CDDP and vehicle. (B) The RTV (relative tumor volume) (\pm SEM) is graphed with error bars representing the standard deviation. (C) The average body weights (\pm SEM) were plotted after sacrifice of the mice treated with **26**, **20**, CDDP and vehicle.

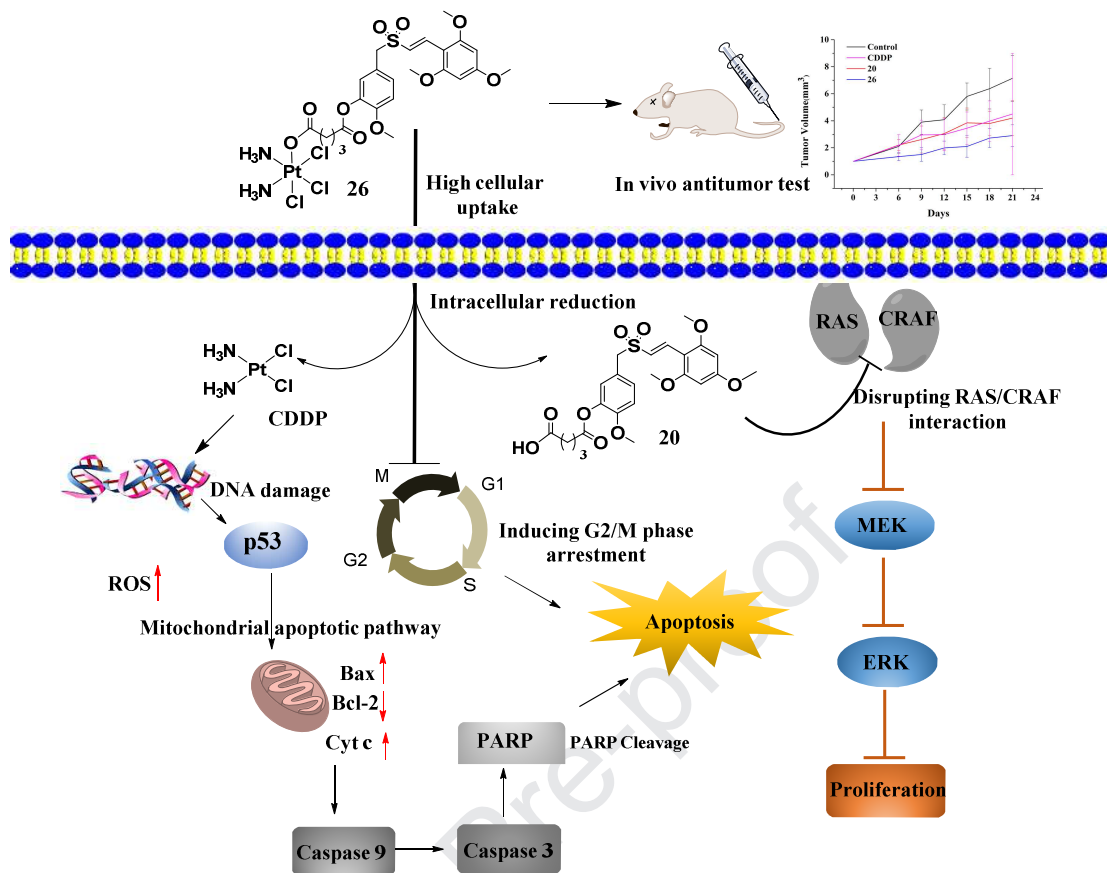


Figure 13. The proposed multifunctional anti-tumor mechanism of 26.

Highlights

- ▶ High cytotoxicity against A549 cells and CDDP-resistant A549 cancer cells with IC_{50} values at 8 nM and 9 nM, respectively.
- ▶ **26** could disrupt RAS-RAF signaling pathway and significant binding ability to CRAF with K_d value of 3.93 μ M.
- ▶ Inducing DNA platination formation.
- ▶ High potency to induce apoptosis through a mitochondrion-dependent pathway.
- ▶ Excellent antitumor activity in xenograft mouse model with good safety profile.

Declaration of interests

The authors declare that they have no known competing financial interests or personal relationships that could have appeared to influence the work reported in this paper.

The authors declare the following financial interests/personal relationships which may be considered as potential competing interests: